Genome Medicine

RESEARCH

Open Access

Pathological mechanisms and candidate therapeutic approaches in the hearing loss of mice carrying human *MIR96* mutations

Morag A. Lewis[1*], Maria Lachgar-Ruiz[1], Francesca Di Domenico[1], Graham Duddy[2], Jing Chen[1], Sergio Fernandez[3], Matias Morin[3], Gareth Williams[1], Miguel Angel Moreno Pelayo[3] and Karen P. Steel[1]

Abstract

Background Progressive hearing loss is a common problem in the human population with no effective therapeutics currently available. However, it has a strong genetic contribution, and investigating the genes and regulatory interactions underlying hearing loss offers the possibility of identifying therapeutic candidates. Mutations in regulatory genes are particularly useful for this, and an example is the microRNA miR-96, a post-transcriptional regulator which controls hair cell maturation. Mice and humans carrying mutations in miR-96 all exhibit hearing impairment, in homozygosis if not in heterozygosis, but different mutations result in different physiological, structural and transcriptional phenotypes.

Methods Here we present our characterisation of two lines of mice carrying different human mutations knocked-in to *Mir96*. We have carried out auditory brainstem response tests to examine their hearing with age and after noise exposure and have used confocal and scanning electron microscopy to examine the ultrastructure of the organ of Corti and hair cell synapses. Bulk RNA-seq was carried out on the organs of Corti of postnatal mice, followed by bioinformatic analyses to identify candidate targets.

Results While mice homozygous for either mutation are profoundly deaf from 2 weeks old, the heterozygous phenotypes differ markedly, with only one mutation resulting in hearing impairment in heterozygosis. Investigations of the structural phenotype showed that one mutation appears to lead to synaptic defects, while the other has a much more severe effect on the hair cell stereociliary bundles. Transcriptome analyses revealed a wide range of misregulated genes in both mutants which were notably dissimilar. We used the transcriptome analyses to investigate candidate therapeutics, and tested one, finding that it delayed the progression of hearing loss in heterozygous mice.

Conclusions Our work adds further support for the importance of the gain of novel targets in microRNA mutants and offers a proof of concept for the identification of pharmacological interventions to maintain hearing.

*Correspondence:
Morag A. Lewis
morag.lewis@kcl.ac.uk
[1] Wolfson Sensory, Pain and Regeneration Centre, King's College London, Guy's Campus, London SE1 1UL, UK
[2] Wellcome Sanger Institute, Hinxton CB10 1SA, UK
[3] Servicio de Genética, Hospital Universitario Ramón y Cajal, IRYCIS and Biomedical Network Research Centre On Rare Diseases (CIBERER), Km 9.100, Madrid 28034, Spain

Background

Progressive hearing loss is a common problem in the human population, but as yet there are no therapeutic treatments available. Part of the reason for this is that adult-onset hearing loss is a highly heterogeneous condition, and many factors can underlie an individual's hearing impairment. However, it is known that there is a considerable genetic contribution [1–3], suggesting

© The Author(s) 2024. **Open Access** This article is licensed under a Creative Commons Attribution 4.0 International License, which permits use, sharing, adaptation, distribution and reproduction in any medium or format, as long as you give appropriate credit to the original author(s) and the source, provide a link to the Creative Commons licence, and indicate if changes were made. The images or other third party material in this article are included in the article's Creative Commons licence, unless indicated otherwise in a credit line to the material. If material is not included in the article's Creative Commons licence and your intended use is not permitted by statutory regulation or exceeds the permitted use, you will need to obtain permission directly from the copyright holder. To view a copy of this licence, visit http://creativecommons.org/licenses/by/4.0/.

that a better understanding of the genes involved may lead to useful pathways to explore therapeutically.

Mutations affecting the microRNA miR-96 have been found to cause progressive hearing loss in humans and in mice [4–6]. MicroRNAs are small noncoding RNA genes which target mRNA molecules through binding to target sites in their 3′UTR and recruiting the RNA-induced silencing complex to downregulate translation (reviewed in [7, 8]). Two of the point mutations of *MIR96* that have been reported in humans cause dominant, progressive hearing loss in carriers [5], both affecting the seed region of the microRNA, which is critical for correct binding to its target mRNA molecules [9]. In the mouse, a third point mutation of the seed region in $Mir96^{Dmdo}$ results in delayed maturation of sensory hair cells in heterozygous carriers, and a complete failure of hair cells and their innervation to develop properly in homozygotes, both in the peripheral and central auditory system [4, 10, 11]. Because of the similarity of the phenotype resulting from these three point mutations, the mechanism of action initially was thought to be the failure to downregulate the normal targets [4, 5]. However, more recent studies on mice carrying null alleles of either *Mir96* and the nearby *Mir183* [12] or of all three microRNAs of the *Mir183* family (*Mir96*, *Mir183* and *Mir182*) [13, 14] found that heterozygous carriers of the null alleles have no hearing phenotype, suggesting that the gain of novel targets due to the changed seed sequence resulting from point mutations is important in the *Mir96* mutant phenotype, not just the loss of normal targeting. Transcriptome analyses of the $Mir96^{Dmdo}$ mutant organ of Corti showed that miR-96 controls a broad regulatory network [15], suggesting that a better understanding of the core genes—particularly the direct targets of miR-96—may suggest candidate therapeutic targets.

Here we present data from mice carrying the two seed region point mutations reported in human families [5]. Both mutations result in profound deafness in homozygotes, but the heterozygote phenotype differs, further supporting the importance of the gain of novel targets in microRNA mutant phenotypes. We have investigated the structural and transcriptomic changes and found evidence for the involvement of different pathological mechanisms; one mutation appears to affect the synapses while the other has a more severe effect on the hair bundle. Finally, we have demonstrated the potential for use of these data to identify candidate therapeutics, and we have tested and confirmed the effect of one such candidate to delay the progression of hearing loss seen in heterozygotes.

Methods

Ethics statement

Mouse studies were performed in compliance with UK Home Office regulations and the Animals (Scientific Procedures) Act of 1986 (ASPA) under UK Home Office licencing, and the study was approved by the King's College London Ethical Review Committee. Mice were culled using methods permitted under these licences to minimise any possibility of suffering.

Husbandry

Mice were housed in groups of up to 5 adults of a single sex, in individually ventilated cages (Tecniplast) with Datesand Aspen bedding. Each cage was provided with environmental enrichment (cardboard tubes and extra nesting material), and the mice had free access to food (LabDiet PicoLab Rodent Diet 20, St. Louis, MO, USA) and water. The temperature was controlled at 21 ± 2 °C, and the humidity at 55 ± 10%, and a 12-h light/dark cycle was maintained throughout the study. Each mouse was checked daily for signs of ill health. Ear biopsies were taken at a minimum age of 10 days old for identification and genotyping. The methods of euthanasia were cervical dislocation for adult mice and decapitation for 4-day-old pups.

Mouse generation and maintenance

Mir96 mutant mice were generated by the Mouse Genetics Project at the Wellcome Sanger Institute by inserting targeted mutations in mouse ES cells in a C57BL/6N genetic background, after which the selection cassette was removed using Flp recombinase. The mouse lines used are $Mir96^{tm2.1Wtsi}$ (hereafter referred to as $Mir96^{+13G>A}$, corresponding to human family s403 [5, 16], ES cell line BEPD0019_D04) and $Mir96^{tm3.1Wtsi}$ (hereafter referred to as $Mir96^{+14C>A}$, corresponding to human family s1334 [5], ES cell line BEPD0003_D07) (Fig. 1). Both mouse lines will be available through the European Mouse Mutant Archive (EMMA). Both colonies were generated and maintained on a C57BL/6N genetic background and were maintained by heterozygous intercrosses or homozygotes crossed with heterozygotes, and both mutant lines produce viable and fertile homozygous offspring. For the testing of the $Mir96^{+13G>A}$ allele on the C3HeB/FeJ background, $Mir96^{+13G>A}$ homozygotes were crossed to C3HeB/FeJ mice, producing F1 mice which were heterozygous on a 50% C3HeB/FeJ, 50% C57BL/6N background. These F1 mice were then bred together, and ABR measurements were taken from their F2 offspring (wildtype, heterozygous and homozygous for the $Mir96^{+13G>A}$ allele, on a 50% C3HeB/FeJ, 50% C57BL/6N background).

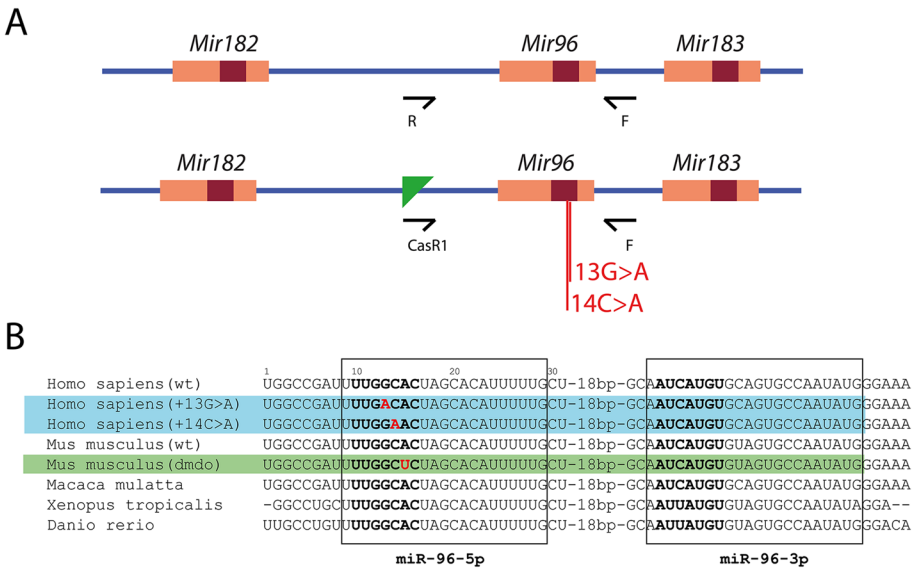

Fig. 1 Schematic showing the allele structure of the mice used in this work. **A** Allele structure and primer location for the wildtype (top) and mutant (bottom) alleles. *Mir96* is one of three microRNAs in the *Mir-183/96/182* gene cluster. Maroon boxes indicate the sequences encoding the seed regions, and the position of the mutations is labelled. Arrows indicate the location and orientation of the primers used for genotyping. Green triangle: FRT site. Not to scale. **B** Partial sequence of the *Mir96* stem-loop showing the point mutations associated with deafness in mice and humans; the sequence shown is from the start to the end of the human gene sequence but not all the species share the same start and end points. The boxes indicate the mature microRNA sequences. The seed region, critical for the correct identification of target mRNAs, is shown in bold. Mutations are shown in red. The two human mutations carried by the $Mir96^{+13G>A}$ and $Mir96^{+14C>A}$ mutants are highlighted in blue; the numbers refer to the position from the start of the human gene. The sequence of *Mir96* with the point mutation in the $Mir96^{Dmdo}$ mouse is highlighted in green [4, 5]

Genotyping

$Mir96^{+13G>A}$ and $Mir96^{+14C>A}$ mice were genotyped by PCR using template DNA extracted from tissue. The mutant allele was amplified using a gene-specific forward primer (5′-CTCACCCCTTTCTGCCTAGA-3′) paired with a reverse primer designed against the remaining FRT site left after removal of the selection cassette (5′-TCGTGGTATCGTTATGCGCC-3′). The wildtype allele was genotyped in a similar way using the same forward primer combined with a reverse primer specific for the wildtype allele (5′-CCTAAGGTAAGCCACTGATGG-3′). The resulting band sizes were 588 bp for the wildtype product and 587 bp for the mutant product. The location of the primers with respect to *Mir96* and the cassette is shown in Fig. 1.

Auditory brainstem response

The hearing of wildtype and mutant $Mir96^{+13G>A}$ and $Mir96^{+14C>A}$ mice was tested using the auditory brainstem response (ABR) as described in [17]. Briefly, mice were sedated using a ketamine/xylazine mix (10 mg ketamine and 0.1 mg xylazine in 0.1 ml per 10 g body weight), and responses were recorded from three subcutaneous needle electrodes. The reference electrode was placed over the left bulla, the ground over the right bulla, and the active electrode was placed on the top of the head. Responses were recorded from 256 stimulus presentations per frequency (broadband click and 3 kHz, 6 kHz, 12 kHz, 18 kHz, 24 kHz, 30 kHz, 36 kHz and 42 kHz pure tone frequencies at sound levels from 0 to 95 dB, in 5 dB steps). Mice were then recovered using atipamezole (0.01 mg atipamezole in 0.1 ml per 10 g body weight). The threshold for each frequency is the lowest intensity at which a waveform could be distinguished, and this was identified using a stack of response waveforms.

Noise exposure

Eight-week-old heterozygous and wildtype $Mir96^{+13G>A}$ mice on the original C57BL/6N genetic background were subjected to 8–16 kHz octave-band noise at 100 dB SPL for 1 h while awake and unrestrained in separate compartments within an exposure chamber set up to provide a uniform sound field [18], as described in [12, 19]. ABRs were carried out 1 day prior to noise exposure, and 1 day, 3 days, 7 days, 14 days and 28 days after exposure. Sham controls were littermates who spent the same time in the exposure chamber without the noise and went through the same set of ABR measurements at the same time.

Scanning electron microscopy

The cochleae of wildtype, heterozygous and homozygous mice at postnatal day (P)28 were collected and fixed for 2 h in 2.5% glutaraldehyde in 0.1 M sodium cacodylate buffer with 2 mM $CaCl_2$. Samples were then fine dissected in PBS to expose the organ of Corti and processed according to the osmium tetroxide-thiocarbohydrazide (OTOTO) method [20] before dehydration through an ethanol series, critical point drying and mounting. Samples were gold-coated to 4 nm thickness. Regions of the cochlea were identified using the frequency-place map described by [21]. Images were taken using a JEOL JSM 7800 Prime scanning electron microscope. A standard magnification of 60×was used to view the whole length of the organ of Corti, and higher magnifications were used for close-ups on hair cell rows (2000×) and individual hair cells (15,000–23,000×). Minimal adjustments were carried out in Adobe Photoshop to normalise dynamic range across all panels.

Whole-mount dissection and immunohistochemistry

The cochleae of 4-week-old mice were fixed in 4% paraformaldehyde (PFA) for 2 h at room temperature (RT). After washing in PBS, samples were decalcified by overnight incubation with 0.1 M EDTA (ethylenediaminetetraacetic acid) disodium salt (Reagecon, cat. no. ED2015) at RT. Following dissection of the organ of Corti, samples were permeabilised with 5% Tween in PBS for 30 min and blocked with 0.5% Triton X-100 and 10% Normal Horse Serum (NHS) in PBS for 2 h at RT. The samples were incubated with the primary antibodies diluted in a 1:2 blocking solution in PBS overnight at 4 °C.

Mir96$^{+13G>A}$ and *Mir96*$^{+14C>A}$ samples were stained for the presynaptic marker C-terminal-binding protein 2 (CTBP2), the postsynaptic marker glutamate receptor 2 (GRIA2 (GluR2)) and the hair cell marker MYO7A. The primary antibodies used were rabbit anti-Myosin VIIa (1:200, 25–6790, Proteus), mouse IgG2 anti-GluR2 (diluted 1:2000, MAB397, Emd Millipore) and mouse IgG1 anti-CtBP2 (diluted 1:200, 612,044, BD Transduction Laboratories). The day after, samples were washed three times with PBS and incubated for 1 h with the secondary antibodies Alexa Fluor 647-conjugated chicken anti-rabbit (1:200, #A21443, Life Technologies), Alexa Fluor 488-conjugated goat anti-mouse (IgG2a) (diluted 1:1000, #A21131, Life Technologies) and Alexa Fluor 568-conjugated goat anti-mouse (IgG1) (1:1000, #A21124, Life Technologies). This step was followed by a second incubation under the same conditions with fresh secondary antibody. Finally, specimens were rinsed with PBS and mounted using ProLong Gold Antifade Mountant with DAPI (P36931, Life Technologies) and stored at 4 °C.

Confocal imaging, synapses and hair cell quantification

Samples were imaged with a Zeiss Imager 710 confocal microscope interfaced with ZEN 2010 software. All images were captured with the plan-Apochromat 63x/1.4 and 40x/1.4 Oil DIC objectives. Overview images of all samples were captured using a lower magnification (×10) to image all pieces of the whole organ of Corti for frequency-place mapping. The Fiji Measure_line plugin [22] was used to map cochlear length to cochlear frequencies. This plugin is based on the mouse tonotopic cochlear map described by Müller and colleagues [21].

To image the synaptic puncta in *Mir96*$^{+13G>A}$ and *Mir96*$^{+14C>A}$ samples, two non-overlapping images were acquired at the 12 kHz best-frequency region. A 2.0 optical zoom was used and a z-step of 0.25 µm was used to ensure that all synaptic puncta were imaged. Images containing puncta were merged in a z-stack and the z-axis maximum intensity projection was used to quantify synapses, which were defined as the colocalisation of CtBP2 and GluR2-labelled puncta. Synapse quantification was performed manually using the cell counter plugin in Fiji. The total number of ribbon synapses was divided by the number of inner hair cells (IHCs) present in the image (Myo7a-labelled) to determine the number of ribbon synapses per IHC. In the cases where an IHC was only partially visible in the image, the synapses corresponding to that cell were not counted.

Reverse transcription and quantitative PCR (RT-qPCR)

The organs of Corti of postnatal day (P)4 mice were dissected and stored at − 20 °C in RNAprotect Tissue Reagent (RNAlater®) (QIAGEN, cat. no. 76106). Total RNA was extracted using the SPLIT RNA extraction kit (Lexogen) according to the manufacturer's instructions, quantified in a Nanodrop spectrophotometer and normalised to the same concentration within each litter. SuperScript™ VILO™ cDNA Synthesis Kit (Thermo Fisher Scientific, cat. no. 11754050) was used for DNase treatment and cDNA synthesis according to the manufacturer's instructions.

Quantitative RT-PCR was performed in a CFX Connect Real-Time PCR Detection System (Bio-Rad Laboratories, Cat. No. 1855201) using TaqMan probes [Applied Biosystems: *Hprt* (Mm01545399_m1), *Prox1* (Mm00435971_m1), *Ocm* (Mm00712881_m1) and *Slc26a5* (Mm01167265_m1)] and SsoAdvanced Universal SYBR Green Supermix (Bio-Rad, #1,725,284). Three technical replicates of each sample and probe were carried out. The number of biological replicates (mice) tested per probe is indicated in the figure legends.

Relative expression levels were calculated using the $2^{-\Delta\Delta CT}$ method [23]. The calibrator was the wildtype littermate C_t for the same probe, with *Prox1* as an internal

control for sensory tissue, because it is expressed in supporting cells [24].

RNA-seq and data analysis

Cochleae were dissected and RNA was extracted from the organ of Corti as described above. Six sex-matched wildtype and homozygous mutant littermate pairs were analysed. Samples were collected within the same 1.5 h time window (from 6 h after lights on) to control for the effects of circadian rhythms on gene expression. The age selected for RNA-seq was postnatal day 4 (P4), as it had been previously described that hair cells are still present at P4 in *Mir96*^{Dmdo} mice, and to allow comparison with previous transcriptomic data from *Mir96*^{Dmdo} [4, 12]. The RNA was extracted using the SPLIT RNA extraction kit (Lexogen) according to the manufacturer's instructions. RNA was quantified using the Qubit RNA HS Assay Kit (Thermo Fisher Scientific Cat.#Q32855) and its quality was assessed on Agilent RNA 6000 Nano or Pico Chips (Agilent Technologies, Cat.# 5067–1511 or Cat.# 5067–1513) before proceeding to library preparation.

Library generation and sequencing were performed at the Center for Cooperative Research in Biosciences (CIC bioGUNE; Madrid) following the "TruSeq Stranded mRNA Sample Preparation Guide" with the corresponding kit [Illumina Inc. Cat.# RS-122–2101 or RS-122–2102] and sequenced on an Illumina HiSeq 4000 machine as paired-end 101 bp reads.

RNA-seq data were analysed using an in-house designed pipeline, as follows. Raw data were pre-processed to mask undetermined nucleotides based on quality using the FastX Toolkit [25] and Trimmomatic 0.39 for adapter trimming based on the sequence. Hisat 2.1.0 [26] was used to align the reads against the GRCm39 reference genome. The Samtools package was used for SAM to BAM conversion [27] and the count matrixes were generated by htseq v0.11.2 [28]. Finally, the edgeR package [29] was used to perform a generalised linear model likelihood ratio test. The resulting gene lists, including differential expression between homozygotes and wildtype samples and false discovery rate, are shown in Additional files 1 and 2: Tables S1 and S2; all genes are included in these lists.

To study the direct effect of the mutant miR-96 on the transcriptomes of the homozygous mutants, we used Sylamer [30], which plots over- and underrepresentation of nucleotide words of specific length within the 3′ untranslated regions (UTRs) of a gene list, in our case the lists presented in Additional files 1 and 2: Tables S1 and S2, ranked in order from most upregulated to most downregulated. To study the indirect effects, we used gene set enrichment analysis (GSEA), to compare the transcriptomes to previously defined gene sets and identify any enrichment in either genotype [31, 32]. The GSEA Preranked option (GSEA v4.3.2) was used to run the gene set enrichment analysis against the lists of differentially expressed genes ranked by $\log_2$ fold change ($\log_2$FC) (ordered from the most upregulated to the most downregulated genes in the homozygote samples) and to determine whether any gene sets were enriched at either end of our ranked gene list. The gene sets used in this study were hallmark gene sets, canonical pathways gene sets derived from the Reactome pathway database, regulatory targets gene sets (potential targets of regulation by transcription factors or microRNAs) and gene ontology gene sets (biological processes, BP; cellular components, CC; and molecular function, MF). All the gene sets were downloaded from the Molecular Signature Database [33], a collection of annotated gene sets for use with GSEA software.

The GSEA output was uploaded into Cytoscape for visualisation and interpretation of enrichment analysis results using the tools EnrichmentMap for network visualisation and WordCount and AutoAnnotate for interpretation and to define the major biological clusters, as described in [34].

Amitriptyline delivery

200 µg/ml amitriptyline hydrochloride (Abcam, cat. no. ab141902) was provided in drinking water with 2% w/v saccharin sodium salt hydrate (Scientific Laboratory Supplies, cat. no. s1002-1 kg) to increase palatability, as described in [35]. Mice were first moved to saccharin in drinking water, then after acclimatisation, they were moved to amitriptyline with the saccharin content kept the same. Control mice were maintained on the saccharin-only water. Their body weight was monitored daily to ensure they remained healthy during acclimatisation. They were then set up in breeding pairs. Offspring were maintained on the same water as their parents for ABR testing up to 6 months old.

Statistical analyses

A one-way ANOVA with Tukey's correction for multiple comparisons was used to compare the three different experimental groups (homozygotes, heterozygotes and wildtypes) in the *Mir96*$^{+13G>A}$ and *Mir96*$^{+14C>A}$ synapse quantification and to generate multiplicity-adjusted *p* values. Ten to 14 hair cells were counted in each frequency region.

For the qPCR, wildtype and homozygote groups were compared using the Wilcoxon rank sum test, because it is a suitable test for small sample sizes and populations of unknown characteristics [36].

ABR data were first transformed using the arcsine transformation, and then analysed as described in [12].

This analysis uses separate linear models for each frequency with a compound symmetric covariance structure and restricted maximum likelihood estimation [37] and permits the inclusion of all data, unlike the repeated measures ANOVA, which cannot include partial data (for example, if a mouse dies before completion of the full set of ABR measurements) [38]. For each stimulus, the interaction of all variables was measured (genotype and age, and noise and drug administration where relevant), followed by Bonferroni correction for multiple testing, using SPSS v25 (IBM).

False discovery rate (FDR)-corrected *p* values were calculated for the RNA-seq data by applying the Benjamini–Hochberg method to the *p* values generated by edgeR [29].

Results

Mir96$^{+13G>A}$ heterozygous mice have normal hearing while *Mir96*$^{+14C>A}$ heterozygous mice exhibit progressive hearing loss

Auditory brainstem response (ABR) recordings showed that *Mir96*$^{+13G>A}$ and *Mir96*$^{+14C>A}$ homozygotes exhibit profound deafness at all ages tested, showing no response at the highest sound level tested (95 dB sound pressure level (SPL)) at any of the ages studied (14 days to 6 months old) (Fig. 2). *Mir96*$^{+14C>A}$ heterozygous mice have mild progressive hearing loss most pronounced at high frequencies and progressing with age to lower frequencies (Fig. 2B), which correlates with the human phenotypes [5, 16]. However, *Mir96*$^{+13G>A}$ heterozygous mice have normal hearing up to 6 months old (Fig. 2A), which does not mimic the phenotype of humans with the equivalent mutation in heterozygosis [5, 16].

The mice were generated and maintained on the C57BL/6N genetic background. C57BL/6N mice are known to have age-related hearing loss, which is caused in part by the *Cdh23*^{ahl} allele [39]. At 4 weeks of age, the high frequencies are affected, whereas the lower frequencies remain unaffected up to 6 months of age [40]. We observed a similar pattern in wildtype mice from the *Mir96*$^{+13G>A}$ and *Mir96*$^{+14C>A}$ lines, which showed mild hearing loss at 24–42 kHz from 8 weeks old, but retained good low-frequency hearing sensitivity up to 6 months old (Fig. 2).

Mir96$^{+13G>A}$ heterozygotes have normal waveforms and retain normal hearing on a different genetic background and when subjected to noise

In order to further investigate the hearing of *Mir96*$^{+13G>A}$ heterozygotes, we first plotted their waveforms at 6 months old and found no obvious difference when compared to the wildtype waveforms (Fig. 3A). Mice were aged to 1 year old, but there was still no difference in the thresholds (Fig. 3B).

Next the hearing of wildtype, heterozygous and homozygous *Mir96*$^{+13G>A}$ mice on a mixed C57BL/6N, C3HeB/FeJ background was tested. The C3HeB/FeJ strain was selected for this outcross because it is known to show good hearing into old age and was the genetic background of the *Mir96*^{Dmdo} mutant line previously studied [4]. However, on the mixed background no difference was found between wildtypes and heterozygotes up to 6 months old, while homozygotes were still profoundly deaf at all ages tested (Fig. 3C).

Finally, *Mir96*$^{+13G>A}$ heterozygote and wildtype mice on the original C57BL/6N background were subjected to 100 dB SPL, 8–16 kHz noise for 1 h to ask if the heterozygotes were more sensitive to noise damage than wildtypes. The noise-exposed mice exhibited a threshold shift which gradually recovered over the subsequent 4 weeks, but there was no obvious difference in thresholds or in threshold recovery rate between the wildtype and heterozygous mice (Fig. 3D). The difference in the mean thresholds of noise-exposed heterozygotes and wildtypes at 30 kHz 14 and 28 days after noise is statistically significant, but there is a lot of variability between individual mice, so we would not conclude that this is a biologically relevant difference. While the *Mir96*$^{+13G>A}$ heterozygous non-exposed mice do appear to have worse thresholds than the non-exposed wildtypes, this is because these five wildtype mice have better high-frequency thresholds than the mice which went through the initial ABR tests (Fig. 2).

Mir96$^{+13G>A}$ and *Mir96*$^{+14C>A}$ homozygous mice have severely affected stereocilia bundles

Scanning electron microscopy (SEM) showed that homozygous mice of either mutation have severely affected stereocilia bundles at postnatal day 28 (P28). Stereocilia defects were seen in both outer hair cells (OHCs) and IHCs and were more severe in *Mir96*$^{+14C>A}$ than in the *Mir96*$^{+13G>A}$ mutants. We observe disorganised stereocilia that had lost their normal staircase arrangement, a fusion of stereocilia, and giant stereocilia, particularly in the IHCs (Fig. 4I, N, O), as well as missing stereocilia bundles (Fig. 4H, K, N). That phenotype becomes more striking at high frequency regions (Additional file 3: Fig. S1).

In the heterozygotes, stereocilia damage is less severe than in the homozygotes. *Mir96*$^{+13G>A}$ heterozygous mice, despite having normal ABR thresholds, show loss of some stereocilia in the shortest row of the OHC bundles, which worsens at higher frequency regions (Fig. 4F). In *Mir96*$^{+14C>A}$ heterozygotes, which have mild hearing loss by P28, some OHC stereocilia bundles have a U-shape,

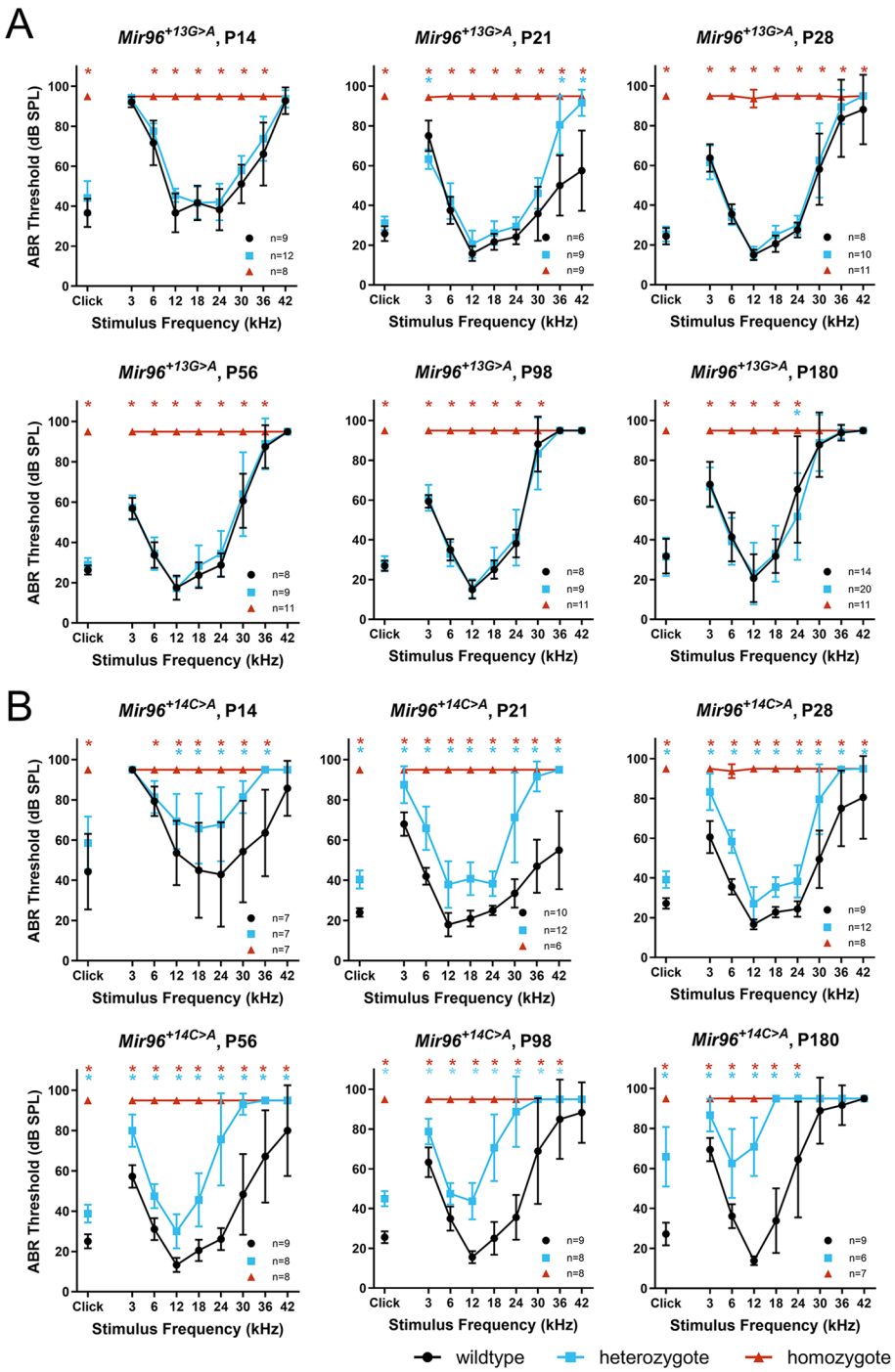

Fig. 2 ABR thresholds of *Mir96*$^{+13G>A}$ (**A**) and *Mir96*$^{+14C>A}$ (**B**) mice at ages from postnatal day (P)14 to P180. ABR measurements in response to click stimuli and tone pips ranging from 3 to 42 kHz were recorded from anaesthetised mice at different ages from P14 to P180. Homozygous mice for either mutation are shown as red triangles, heterozygotes as blue squares, and wildtypes as black circles. Each point in the plot shows the mean of the lowest stimulus level (threshold) at which a response is observed, ± SD. Points at 95 dB sound pressure level (SPL) indicate that there is no response up to the maximum sound level used. Both males and females were tested and are plotted together; *n* numbers are shown on each plot. Asterisks indicate significant differences (Bonferroni-corrected $p < 0.05$, mixed linear model pairwise comparison) between heterozygous mice and wildtypes (blue) or homozygous mice and wildtypes (red)

instead of the typical V-shape observed in wildtypes; this rounding is more often seen towards the apical turn of the cochlea (Fig. 4M). In inner hair cells of *Mir96*$^{+14C>A}$ heterozygotes, some of the stereocilia appeared to taper towards their tips (Fig. 4L).

Mir96$^{+13G>A}$ homozygous mice show a reduction in the number of IHC synapses

Confocal microscopy was used following immunolabelling of the pre- and postsynaptic markers CTBP2 and GRIA2 (GluR2), respectively, to study the synapses at 4 weeks old (Fig. 5A). *Mir96*$^{+13G>A}$ homozygotes were found to have a significant reduction in the number of ribbon synapses (defined as colocalised pre- and postsynaptic labelling) per inner hair cell compared to wildtypes at 4 weeks old (Fig. 5B). There were no differences in heterozygotes compared to wildtypes. Furthermore, no significant differences were found in the number of synapses in *Mir96*$^{+14C>A}$ wildtypes, heterozygotes and homozygotes (Fig. 5C).

Ocm and *Slc26a5* are downregulated in *Mir96*$^{+13G>A}$ and *Mir96*$^{+14C>A}$ homozygotes

Ocm and *Slc26a5* are two genes that are strongly expressed in normal outer hair cells and both were strongly downregulated in *Mir96*^{Dmdo} mice [4] and in *Mir183/96*^{dko} mice [12]; neither are predicted targets of miR-96, nor of any of the mutant miR-96 forms. Therefore, we measured expression levels of these two genes in the two new mutants studied here using qPCR on RNA from the organ of Corti at P4, and both genes were found to be significantly downregulated in *Mir96*$^{+13G>A}$ and *Mir96*$^{+14C>A}$ homozygotes (Fig. 6).

Mir96$^{+14C>A}$ homozygous mice have a larger number of differentially expressed genes than *Mir96*$^{+13G>A}$ homozygotes

In order to further explore the transcriptome of these mice, we carried out RNA-seq analysis of the organ of Corti of homozygotes and wildtype sex-matched littermates at P4. This age was chosen because earlier analyses had shown that all hair cells were still present at this early age, and we wanted to detect expression changes reflecting the different genotypes of the mice rather than due simply to reduced numbers of the cell type of interest (hair cells). Our results revealed that many genes are significantly dysregulated (FDR < 0.05) in the organ of Corti of *Mir96*$^{+13G>A}$ and *Mir96*$^{+14C>A}$ homozygous mice, confirming that miR-96 controls a complex network of genes in the inner ear (Fig. 7, Additional file 4: Table S3). *Mir96*$^{+13G>A}$ homozygotes have 328 significantly differentially expressed genes (DEGs), 203 of which are upregulated and 125 downregulated. In *Mir96*$^{+14C>A}$ mutants, a total of 693 genes are significantly differentially expressed, with 369 upregulated and 324 downregulated. The much larger number of DEGs in *Mir96*$^{+14C>A}$ homozygous mice compared to *Mir96*$^{+13G>A}$ homozygotes correlates with the more severe structural phenotype observed in these mutants (Fig. 4). The two mutants share only 124 DEGs misregulated in the same direction, indicating that transcriptomic changes due to each mutation are very different, even though both mutations are only one base apart in the *Mir96* sequence (Fig. 7, Additional file 4: Table S3).

Sylamer analysis identifies both loss of wildtype targets and gain of novel targets in each mutant

We used Sylamer [30] to assess the impact of the two mutations on the mRNA profile of both mutants. Sylamer counts the occurrences of all possible heptamers in the 3′UTRs of the genes in the RNA-seq datasets, considered in order from most upregulated to most downregulated, and measures the enrichment of each heptamer throughout the ranked gene list. We found that the complementary heptamer to the miR-96 seed region (GTGCCAA, red line) was greatly enriched in the 3′UTRs of hundreds

(See figure on next page.)

Fig. 3 Further electrophysiological investigation of the *Mir96*$^{+13G>A}$ heterozygous mice. **A** Mean ABR waveforms at 12 kHz, shown at 20 dB (top) and 50 dB (bottom) above threshold (sensation level, SL) ± standard deviation, at 6 months old. There is no obvious difference in waveform between *Mir96*$^{+13G>A}$ heterozygous (blue, $n = 20$) and wildtype mice (black, $n = 14$). **B** Mean ABR thresholds from *Mir96*$^{+13G>A}$ homozygous (red triangles), heterozygous (blue squares) and wildtype (black circles) mice at 9 months and 1 year old. Males and females are plotted together; *n* numbers are shown on each plot. **C** Mean ABR thresholds from *Mir96*$^{+13G>A}$ homozygous (red triangles), heterozygous (blue squares) and wildtype (black circles) mice on a mixed C3HeB/FeJ, C57BL/6N background at ages from 3 weeks to 6 months old. Males and females are plotted together; *n* numbers are shown on each plot. For **B** and **C**, asterisks indicate significant differences (Bonferroni-corrected $p < 0.05$, mixed linear model pairwise comparison) between heterozygous mice and wildtypes (blue) or homozygous mice and wildtypes (red). **D** Mean ABR thresholds from *Mir96*$^{+13G>A}$ heterozygous and wildtype mice before and at multiple time points after noise exposure, showing similar recovery of thresholds in wildtype (brown circles, $n = 5$) and heterozygous (purple squares, $n = 5$) mice. Control wildtype (black circles, $n = 5$) and heterozygous (blue squares, $n = 5$) littermates went through the same set of ABR measurements and spent the same time in the noise exposure chamber, but without the noise. Males and females are plotted together. Asterisks indicate significant differences (Bonferroni-corrected $p < 0.05$, mixed linear model pairwise comparison) between unexposed wildtype and unexposed heterozygous mice (blue) or noise-exposed wildtype and noise-exposed heterozygous mice (purple). Error bars in all panels are standard deviation

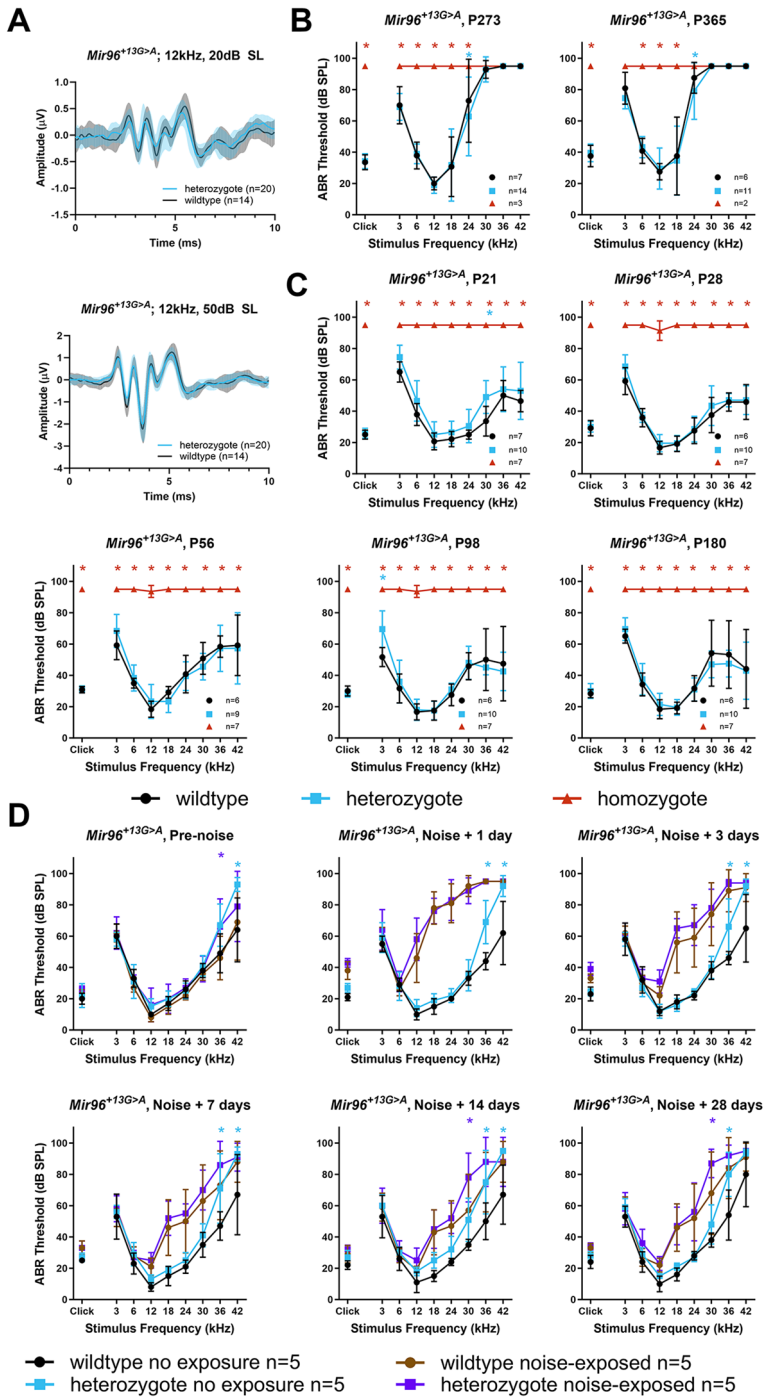

Fig. 3 (See legend on previous page.)

of genes upregulated in *Mir96*$^{+13G>A}$ and *Mir96*$^{+14C>A}$ homozygotes (Fig. 8). This indicates that miR-96 normally represses a wide range of target genes, and when it is mutated, it is not able to repress its targets, which then become upregulated.

We then asked whether mutations led to the silencing of potential acquired targets, that is, those genes containing in their 3′UTR binding sites complementary to the mutant seed region of miR-96. We observed that the heptamer complementary to the mutant miR-96 is

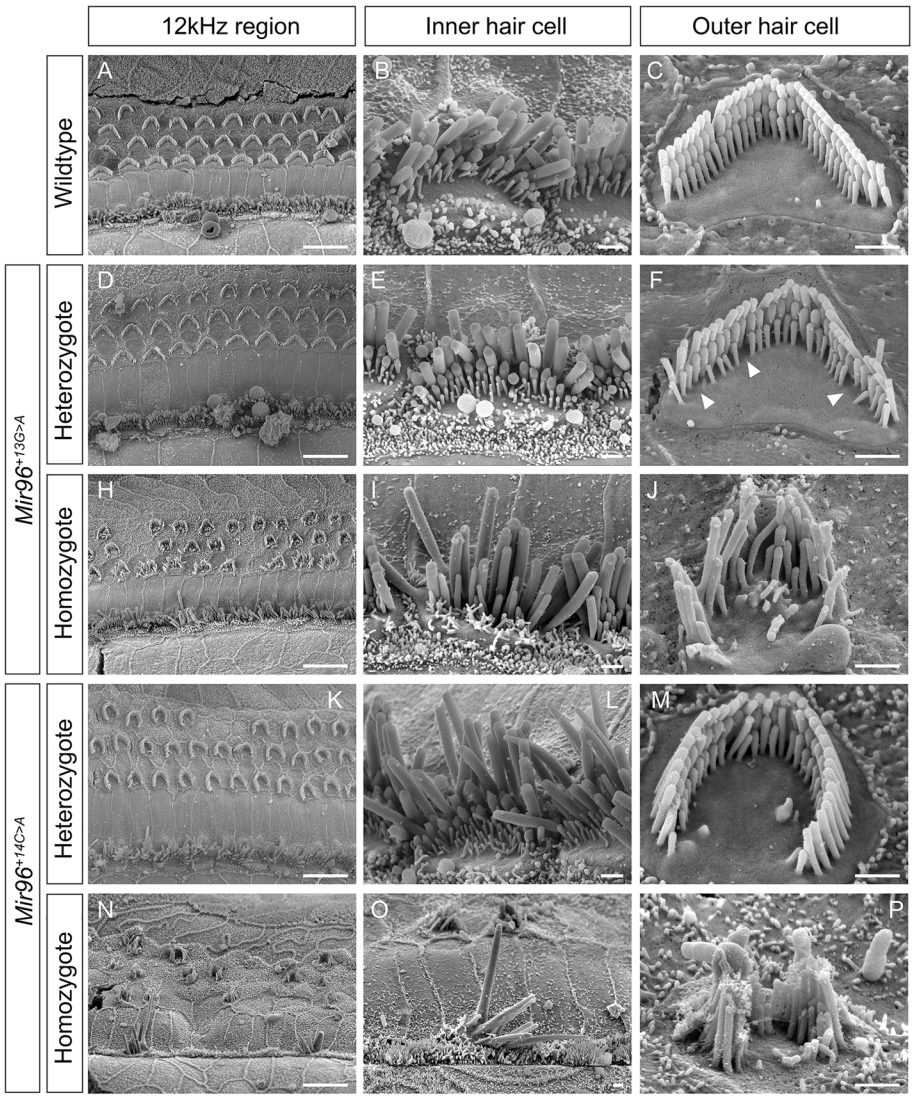

Fig. 4 Scanning electron micrographs of *Mir96*$^{+13G>A}$ (**D**–**J**) and *Mir96*$^{+14C>A}$ (**K**–**P**) mice at 4 weeks old. Representative examples of wildtype (**A**–**C**), heterozygous (**D**–**F**, **K**–**M**) and homozygous (**H**–**J**, **N**–**P**) mice are shown. All images correspond to the 12 kHz best frequency region. For each panel, the left column (**A**, **D**, **H**, **K**, **N**) shows a zoomed-out image with inner and outer hair cell rows. The middle column (**B**, **E**, **I**, **L**, **O**) shows an inner hair cell close up, and the right column (**C**, **F**, **J**, **M**, **P**) shows an outer hair cell close up. *Mir96*$^{+13G>A}$ mice: wildtype ($n=4$), heterozygote ($n=3$), homozygote ($n=3$). *Mir96*$^{+14C>A}$ mice: wildtype ($n=2$), heterozygote ($n=6$), homozygote ($n=3$). Arrowheads in **F** point to the loss of stereocilia in the shortest row of the OHC bundles in *Mir96*$^{+13G>A}$ heterozygotes. Scale bar on left hand panels = 10 µm; scale bar for single hair cells = 1 µm

enriched among the most downregulated genes, indicating that mutant miR-96 influences the expression of newly acquired target genes. The complementary heptamer to the *Mir96*$^{+13G>A}$ mutant seed region is GTG TCAA (Fig. 8, purple line), and the one complementary to the *Mir96*$^{+14C>A}$ mutant seed region is GTTCCAA (Fig. 8, cyan line).

The differentially expressed genes in *Mir96*$^{+13G>A}$ and *Mir96*$^{+14C>A}$ mutants are enriched in specific processes

We carried out gene set enrichment analysis (GSEA) [31, 32] on the transcriptomes from each mutant (Additional file 5: Table S4) and visualised the results in Cytoscape. An enrichment map was generated for each mutant (Additional file 3: Fig. S2) [34]. From the *Mir96*$^{+13G>A}$ enrichment map (Additional file 3: Fig. S2A), we observed that a large number of DEGs were involved in synaptic activity, with terms like "presynaptic", "dopamine transport" and "NMDA activation" being enriched, which correlates with the synaptic phenotype in this mutant (Fig. 5). In the *Mir96*$^{+14C>A}$ network (Additional file 3: Fig. S2B), we observed gene sets involved in functions related to the cytoskeleton, extracellular matrix and adhesion molecules, which may be connected to the

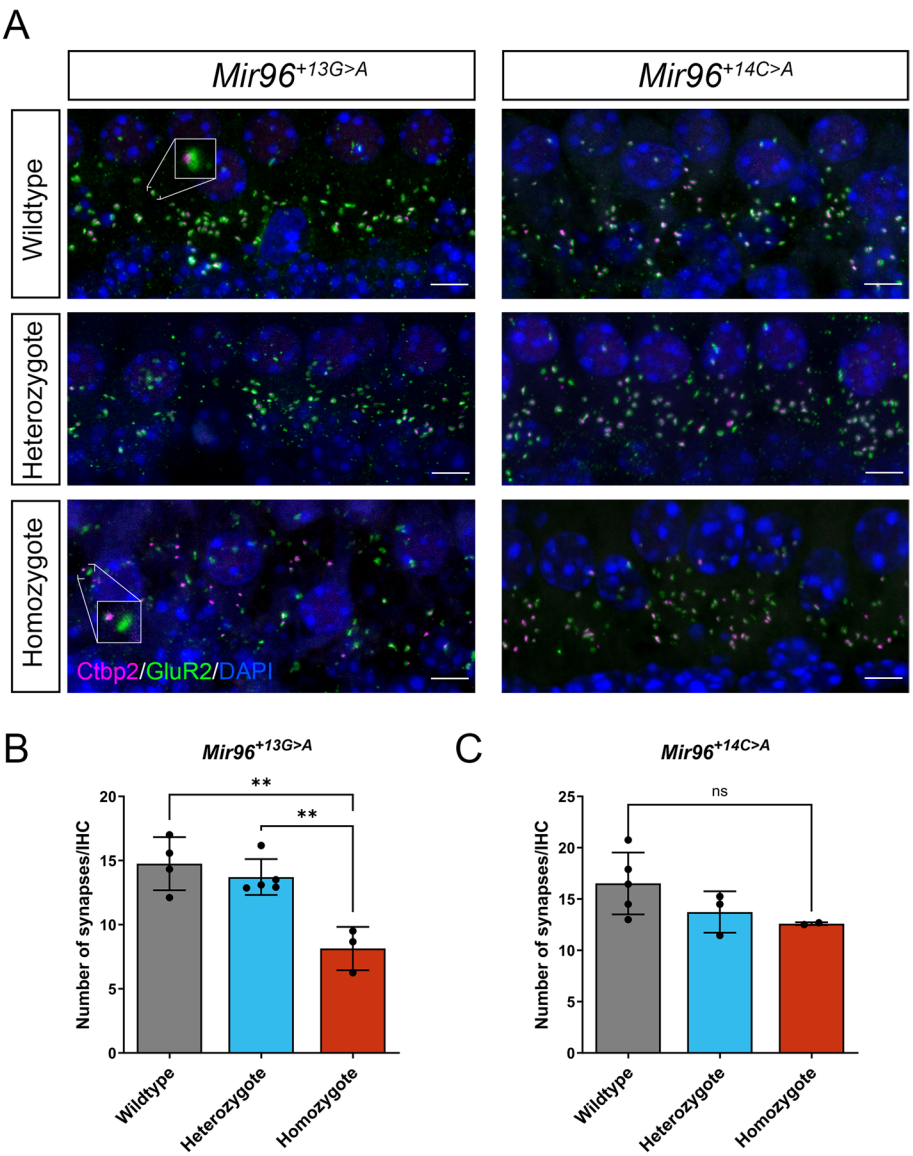

Fig. 5 Analysis of synapses in *Mir96*$^{+13G>A}$ and *Mir96*$^{+14C>A}$ mutant mice at 4 weeks old. **A** Confocal images of the whole-mount organ of Corti. Synapses were examined using an anti-CtBP2 antibody to mark pre-synaptic ribbons (pink) and an anti-GluR2 antibody to mark postsynaptic densities (green). Nuclei are shown in blue (DAPI). The images correspond to the cochlear region of 12 kHz best frequency. Scale bar = 5 µm. Insets in the *Mir96*$^{+13A>G}$ wildtype and homozygote panels show enlarged examples of a colocalised synapse (wildtype) and orphan pre- and postsynaptic labels (homozygote). Quantification of ribbon synapses per IHC in *Mir96*$^{+13G>A}$ (**B**) and *Mir96*$^{+14C>A}$ (**C**). Confocal z-stacks were obtained with a z-step size of 0.25 µm and maximum intensity projection images were used for synapse counting. Colocalised pre- and postsynaptic components were defined as a synapse. Synapses were counted and divided by the number of IHCs, determined by Myo7a staining (not shown in the images, only used for quantification purposes). All data are shown as mean ± SD and statistically analysed by one-way ANOVA with Tukey's multiple comparisons test (** = $p < 0.01$). *Mir96*$^{+13G>A}$ mice: wildtype ($n = 4$), heterozygote ($n = 5$), homozygote ($n = 3$); $p = 0.0016$ (wildtype vs heterozygote adj. $p = 0.65$; heterozygote vs homozygote adj. $p = 0.0041$; wildtype vs homozygote adj. $p = 0.0018$). *Mir96*$^{+14C>A}$ mice: wildtype ($n = 5$), heterozygote ($n = 3$), homozygote ($n = 2$); $p = 0.18$

severe stereocilia degeneration observed in these mice (Fig. 4).

We also analysed the significantly misregulated genes using Ingenuity Pathway Analysis (Qiagen, Germany), which identified canonical pathways with a significant overlap with the misregulated genes. There were 10 pathways with significant overlaps in the *Mir96*$^{+13G>A}$ data, including sensory processing of sound by outer and inner hair cells of the cochlea, and several pathways involved in synaptic activity, correlating with the GSEA analysis

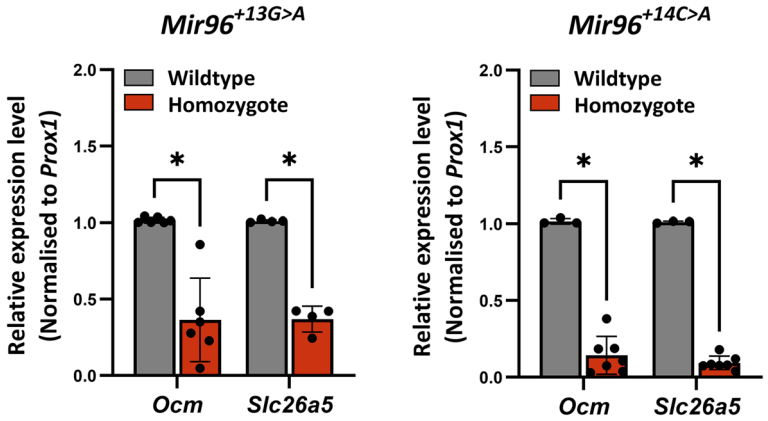

Fig. 6 *Ocm* and *Slc26a5* are downregulated in *Mir96*$^{+13G>A}$ and *Mir96*$^{+14C>A}$ mutants. RT-qPCR was carried out on cDNA from the organ of Corti of P4 wildtype (grey) and homozygous (red) littermates to test gene expression changes. Mean expression levels were calculated from individual expression levels from each mouse and normalised to expression in a wildtype littermate. Relative expression levels were determined using the $2^{-\Delta\Delta ct}$ equation [23], using *Prox1* as an internal control for the amount of organ of Corti tissue present because *Ocm* and *Slc26a5* are specifically expressed in hair cells whereas *Prox1* is expressed in supporting cells of the organ of Corti [24]. Error bars represent the standard deviation (Wilcoxon test; * = $p < 0.05$). *Mir96*$^{+13G>A}$ *Ocm* = 6 wildtypes, 6 homozygotes, $p = 0.0022$; *Slc26a5* $n = 4$ wildtypes, 4 homozygotes, $p = 0.029$. *Mir96*$^{+14C>A}$ *Ocm* = 3 wildtypes, 7 homozygotes, $p = 0.017$; *Slc26a5* $n = 3$ wildtypes, 7 homozygotes, $p = 0.017$. At least three technical replicates were used for each experiment

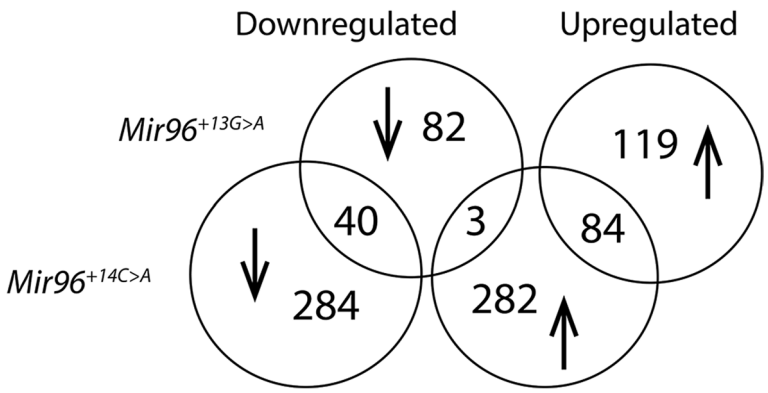

Fig. 7 Comparison of up- and downregulated genes in *Mir96*$^{+13G>A}$ and *Mir96*$^{+14C>A}$ homozygotes. The majority of differentially expressed genes (DEGs) are not shared. Three genes are upregulated in *Mir96*$^{+14C>A}$ and downregulated in *Mir96*$^{+13G>A}$ homozygotes

(Additional file 6: Table S5). From the *Mir96*$^{+14C>A}$ data, we obtained 45 significant pathways, which may reflect the higher number of significantly differentially expressed genes in this mutant dataset. The pathways included sensory processing of sound, degradation of the extracellular matrix, assembly of collagen fibrils and integrin cell surface interactions, which again correlates with the GSEA analysis (Additional file 6: Table S5).

Comparison of the misregulated genes with *Mir96*^{Dmdo} and *Mir183/96*^{dko} mutants

Our aim in investigating the transcriptome of these *Mir96* mutant mice was to determine candidate proteins with therapeutic potential. However, comparison of DEGs in *Mir96*$^{+13G>A}$ and *Mir96*$^{+14C>A}$ with previous data from *Mir96*^{Dmdo} ([15], Additional file 5: Table S4) and *Mir183/96*^{dko} [12] (Fig. 9) revealed only six genes shared between the four mutants. *Myo3a*, *Hspa2* and *St8sia3* are upregulated, while *Tmc1*, *Slc26a5* and *Ocm* are downregulated. Some other genes are differentially expressed in just two or three of the mutants, but most of them are differentially expressed in only a specific mutant, highlighting the transcriptomic differences obtained as a consequence of the different mutations and the different approaches. Furthermore, some genes are misregulated in two or more mutants but in different directions. For example, *Otof* is downregulated in *Mir96*$^{+13G>A}$ and *Mir96*$^{+14C>A}$ mutants, but it is upregulated in *Mir96*^{Dmdo} mice.

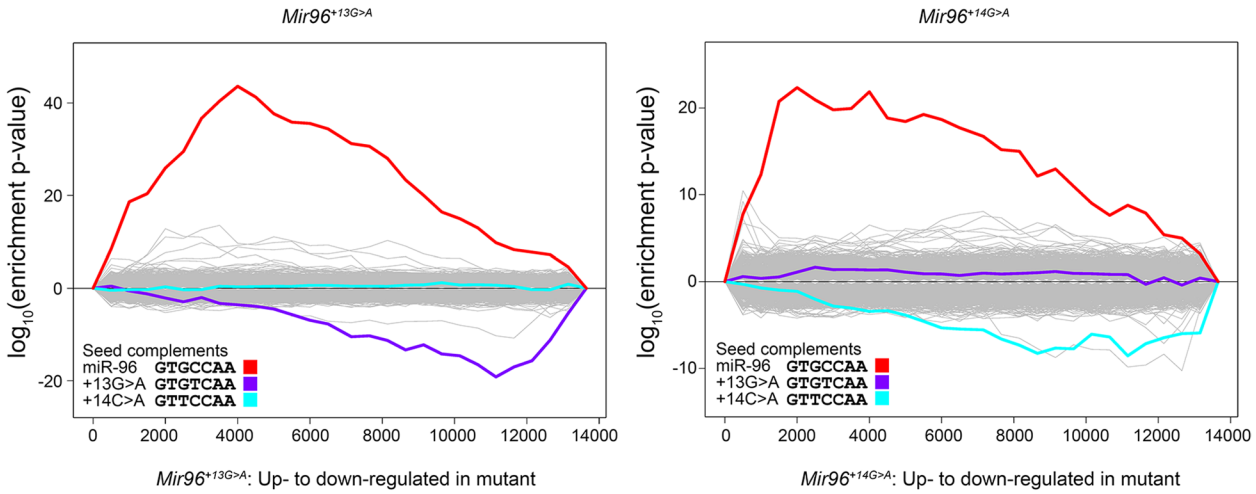

Fig. 8 Sylamer enrichment landscape plots for *Mir96*$^{+13G>A}$ and *Mir96*$^{+14C>A}$ homozygous mice. The plots show enrichment and depletion of heptamers in the 3′UTRs of the differentially expressed genes (DEGs). The x-axis shows the list of DEGs for each mutant ranked from most upregulated (left) to most downregulated (right), based on the fold change (logFC). The Y axis shows the hypergeometric significance for the enrichment or depletion of heptamers in 3′UTRs in the leading parts of the gene list. Positive values indicate enrichment and negative values indicate depletion. The grey lines show the profiles of unenriched heptamers, while the coloured lines represent heptamers that are complementary to the seed regions of wildtype and mutant miR-96. Sylamer measures the enrichment of every possible heptamer in the 3′UTRs of the genes, in cumulative bins of 500 (x-axis), and generates a landscape plot. In this case, the main peaks in both mutants are from the wildtype seed (red) and show that it is enriched in the upregulated genes. The negative peaks on the right hand of each plot indicate that the downregulated genes are enriched in heptamers corresponding to the mutant miR-96. In the *Mir96*$^{+13G>A}$ graph, the purple line corresponds to the mutant seed region, and in the *Mir96*$^{+14C>A}$ graph, the main peak of the mutant seed region is indicated in cyan. These negative peaks suggest that the mutant miR-96 is acquiring new targets. Neither of the mutant seed regions is enriched in the other mutant (cyan line in *Mir96*$^{+13G>A}$, purple line in *Mir96*$^{+14C>A}$)

Identification of candidate miR-96 targets

Identifying targets of a master regulator is an important step in building a network which can then be assessed for therapeutic potential. We took three approaches to investigate potential direct targets of miR-96 in all four mutant mice.

First, we used Sylamer with different word lengths (6, 7 (as above) and 8) and identified the peak enrichment of the wildtype seed region closest to the start of the ranked genes (ranked from most upregulated to most downregulated). Genes ranking higher than this threshold (that is, to the left of this peak, shown by a vertical line in Additional file 3: Fig. S3) whose 3′UTR sequences contain matches to the miR-96 seed region are candidate targets [30] (Additional file 7: Table S6).

Secondly, we used the gene set enrichment analysis to identify gene sets defined by a common regulator, usually identified by the presence of a binding motif close to their start sites. We performed the same GSEA analysis on the *Mir183/96*^{dko} and *Mir96*^{Dmdo} transcriptomes [4, 12] (Additional file 8: Table S7) and tested the identified transcription factors from all four analyses for the presence of wildtype miR-96 seed region matches in their 3′UTRs (Additional file 7: Table S6).

Thirdly, we used Ingenuity Pathway Analysis (IPA) to predict upstream regulators [41] based on the significantly misregulated genes in each of the four mutant miR-96 transcriptomes. From the list of potential upstream regulators, we selected those genes which were predicted to have higher activity in homozygotes and had wildtype miR-96 seed region matches in their 3′ UTRs, and excluded genes known to be downregulated (Additional file 7: Table S6).

Only two proteins were identified as candidates by more than one approach: Pax7 and Atf3, found in both the GSEA and IPA analyses (Additional file 7: Table S6). There were no overlaps between either the GSEA or the IPA target lists and the Sylamer targets.

Identifying candidate therapeutics from whole transcriptome data

Because we were unable to identify a shortlist of candidate target genes or proteins to assess for therapeutic potential, we chose instead to use the whole transcriptome, comparing it to known drug profiles from DrugMatrix, which contains the results from thousands of experiments treating rats or rat cell lines with drugs [42]. This was carried out using the SPIED (Searchable

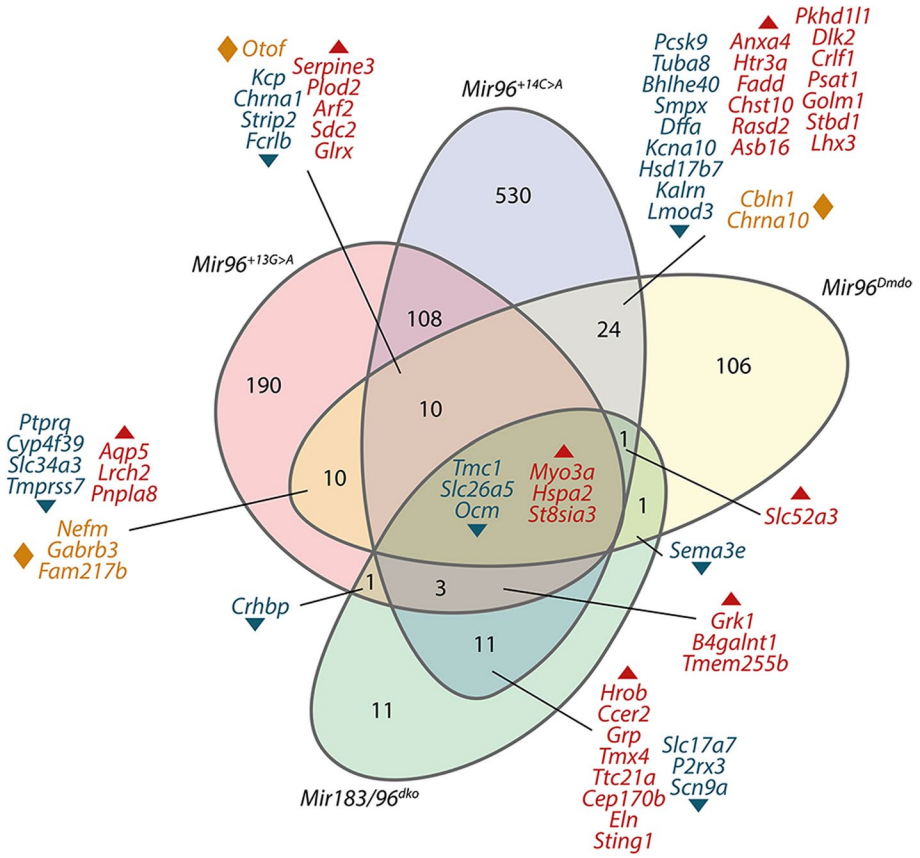

Fig. 9 Comparison of the differentially expressed genes between four miR-96 mutants: *Mir96*$^{+13G>A}$, *Mir96*$^{+14C>A}$, *Mir96*^{Dmdo} and *Mir183/96*^{dko}. Downregulated genes are indicated in dark teal, upregulated genes in red, and genes that are upregulated in one mutant and downregulated in another are shown in orange

Platform-Independent Expression Database) platform [43–45]. In order to focus on the most important differentially expressed genes and to exclude, as much as possible, genes misregulated because they are novel targets of a specific mutant miR-96 seed, we looked at genes with consistent differential expression between the *Mir96*$^{+13G>A}$ and the *Mir96*$^{+14C>A}$ transcriptomes (7944 genes in total, Additional file 9: Table S8). We did not include the other two transcriptomes because they were carried out on different platforms and with different methods, which could result in exclusion of genes for reasons unrelated to their biological relevance (for example, *Ccer2*, which is downregulated in the *Mir183/96*^{dko} and the *Mir96*$^{+14C>A}$ transcriptomes, was not present on the microarray used for the *Mir96*^{Dmdo} study).

SPIED outputs 100 profiles by default, ranked from the most similar to the input profile to the most dissimilar, and the drugs with the most dissimilar profile are potential therapeutics because they lead to a complementary change in transcription patterns across the 7944 genes tested. Among the anti-correlated drug profiles compared with the profiles from *Mir96*$^{+13G>A}$ and *Mir96*$^{+14C>A}$ (Additional file 9: Table S8) is amitriptyline, a tricyclic antidepressant which has previously been reported to improve recovery after noise-induced hearing loss in guinea pigs [46]. Amitriptyline was also identified in the SPIED analysis of the *Mir183/96*^{dko} transcriptome, which should not include novel targets since the mutant allele is a deletion of *Mir96* (Additional file 9: Table S8). It is known to cross the blood–brain barrier [47], which suggests it may also be able to cross the blood-labyrinth barrier. We therefore considered it a good candidate for testing in *Mir96* mutant mice.

Amitriptyline delays hearing loss in *Mir96*$^{+14C>A}$ heterozygotes

We first tested amitriptyline in wildtype C57BL/6N mice to verify that it did not affect hearing and found that at 4 weeks old there was no difference between wildtype mice drinking water with saccharin and wildtype mice drinking water with saccharin and amitriptyline (Additional file 3: Fig. S4). We then tested *Mir96*$^{+14C>A}$ heterozygotes and homozygotes, and wildtype littermates,

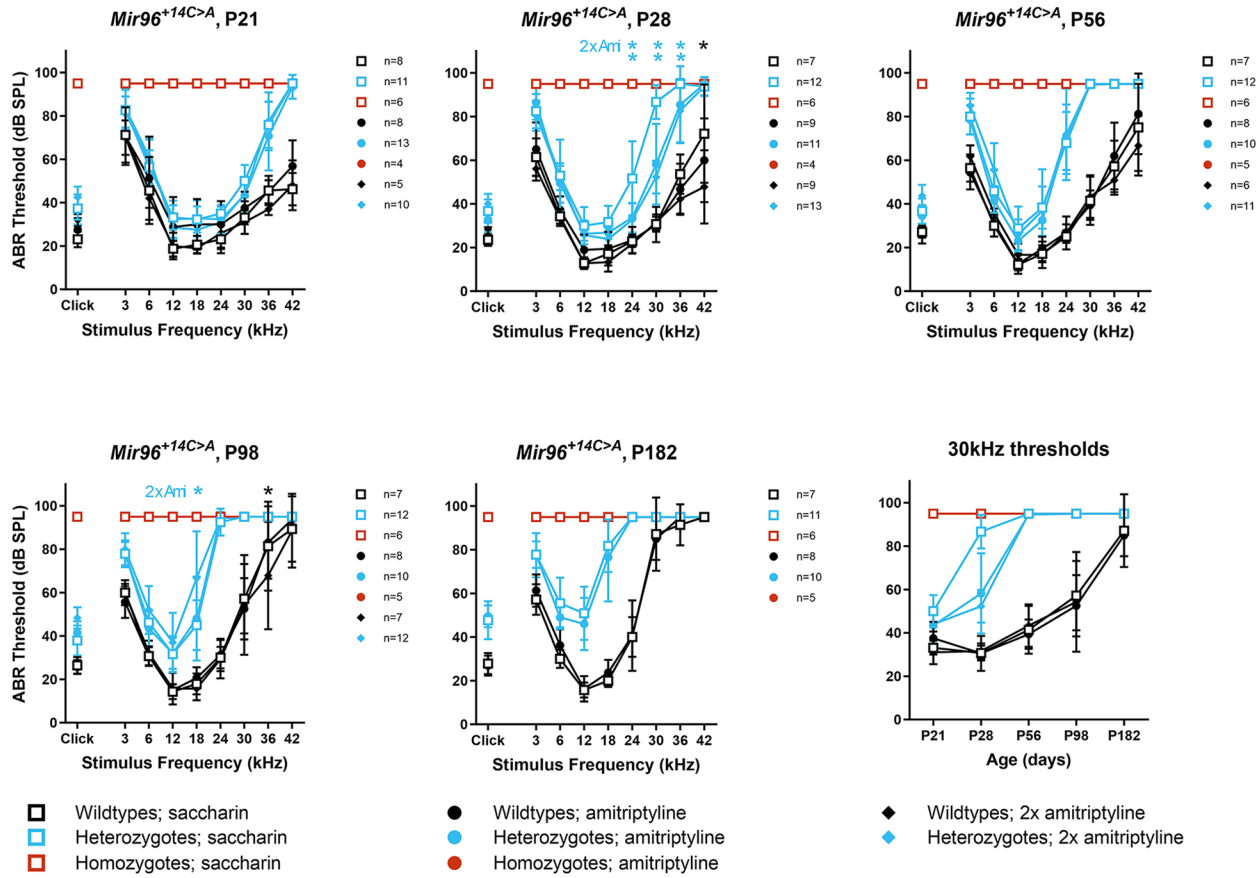

Fig. 10 Amitriptyline delays the progression of hearing loss in *Mir96*$^{+14C>A}$ heterozygotes. Mean ABR thresholds from *Mir96*$^{+14C>A}$ heterozygous mice and wildtype littermates drinking either saccharin (open squares), 200 µg/ml amitriptyline plus saccharin (circles) or 400 µg/ml amitriptyline plus saccharin (diamonds) at ages from 21 days to 6 months. Asterisks indicate significant differences (Bonferroni-corrected $p < 0.05$, mixed linear model pairwise comparison) between mice drinking either amitriptyline or double-dose amitriptyline (2 × Ami) compared to mice of the same genotype drinking saccharin. Significant differences between heterozygotes on differing dosages are marked in blue, and significant differences between wildtypes on different dosages are marked in black. The final plot shows mean thresholds at 30 kHz plotted against time. Error bars are standard deviation

given either saccharin alone, saccharin and 200 µg/ml amitriptyline, or saccharin and 400 µg/ml amitriptyline. We observed progressive hearing loss in the heterozygotes drinking amitriptyline, but it was significantly delayed at high frequencies between 24 and 36 kHz compared to the heterozygotes drinking only saccharin, most visibly at 30 kHz at 4 weeks old (Fig. 10). No improvement was seen in the homozygotes drinking amitriptyline, and increasing the dose of amitriptyline to 400 µg/ml made no difference to the hearing impairment in either heterozygotes or homozygotes (Fig. 10).

Discussion

Comparison with human phenotype and relevance to human *MIR96* mutations

The more severe phenotype observed in mutant mice with a point mutation in the seed region of miR-96 (*Mir96*^{Dmdo}, *Mir96*$^{+13G>A}$ and *Mir96*$^{+14C>A}$) compared to that of mice lacking miR-96 (*Mir183/Mir96*^{dko}) suggests that the gain of novel targets plays an important role in the phenotype caused by miR-96 mutations. This has significant implications for the development of therapies. Since we know that the *Mir183/96*^{dko} heterozygotes have normal hearing, one copy of wildtype miR-96 is enough for normal hearing function. Therefore, the use of a silencing RNA to target only the mutant copy of miR-96 may be enough to allow normal hearing.

While the *Mir96*$^{+14C>A}$ heterozygotes mimic the phenotype observed in the family with the equivalent mutation, the *Mir96*$^{+13G>A}$ heterozygotes escape deafness while the same mutation causes progressive hearing loss in humans [5, 16]. *Mir96*$^{+13G>A}$ heterozygotes do not show raised thresholds up to 1 year old (Fig. 2), in contrast to the progressive hearing loss observed in adulthood in the human counterparts. We tested this allele on a different genetic background and exposed the mice

Table 1 Comparison of the phenotype in the three *Mir96* mutant mice carrying point mutations reported so far, including the two reported in this work, and the *Mir183/96* double knockout. *DEG* differentially expressed gene

	Genotype	*Mir96*^{Dmdo}	*Mir96*$^{+14C>A}$	*Mir96*$^{+13G>A}$	*Mir183/96*^{dko}
Genetic background	All the genotypes	C3HeB/FeJ	C57BL/6N	C57BL/6N	C57BL/6N
Auditory brainstem responses	Heterozygotes	Early onset, rapidly progressive hearing loss	Progressive hearing loss	Normal hearing	Normal hearing
	Homozygotes	Profound deafness	Profound deafness	Profound deafness	Profound deafness
Surface of the organ of Corti	Heterozygotes	Rounded bundles and disorganised stereocilia	Rounded OHC stereocilia bundles	Loss of stereocilia in the innermost row of the OHCs	OHCs have rounded stereocilia bundles. IHCs appear normal
	Homozygotes	Most hair cells have degenerated by 4 weeks old	Most bundles are missing	Severely affected stereocilia bundles	Severely affected IHCs and OHCs stereocilia bundles
Synapses	Heterozygotes	NA	Normal	Normal	Normal
	Homozygotes	Immature IHC ribbon synapses	Normal	Significantly reduced at 4 weeks old	Significantly reduced at 4 weeks old
Transcriptomics, number of DEGs (method)	Heterozygotes	NA	NA	NA	NA
	Homozygotes	86 (microarray)	693 (RNA-seq)	328 (RNA-seq)	34 (RNA-seq)

on the original background to noise, but found no differences in heterozygotes compared with wildtypes (Fig. 3). Therefore, we suggest that the normal hearing observed in *Mir96*$^{+13G>A}$ heterozygous mice compared to the progressive hearing loss observed in humans carrying the same mutation may be due to the repression of different novel target genes in humans and mice. One potential candidate is *RAB11A*, a gene which in humans has three matches to the *Mir96*$^{+13G>A}$ mutant seed region in its 3′UTR. There are no matches to the wildtype seed region, and no matches in the mouse *Rab11a* 3′UTR to either mutant or wildtype seed regions. This gene has recently been reported to be required for correct development of the stereocilia bundle in mice [48]. Identification of this and other candidates could be tested in future studies in cultured cells.

The auditory phenotype of *Mir96*$^{+14C>A}$ mice is more severe than that of *Mir96*$^{+13G>A}$ mice but less severe than that of *Mir96*^{Dmdo} mutants

Mice heterozygous for the *Mir96*$^{+14C>A}$ point mutation exhibit progressive hearing loss from 4 weeks old, while *Mir96*$^{+13G>A}$ heterozygotes have normal ABR thresholds (Fig. 2). *Mir96*^{Dmdo} heterozygous mice (which carry the + 15A > U point mutation) exhibit early-onset rapidly progressive hearing loss, even at 2 weeks old [10]. Initially, it was thought that the *Mir96*^{Dmdo} phenotype was due to haploinsufficiency rather than the acquisition of novel targets because humans heterozygous for different point mutations also have progressive hearing loss [4, 5]. However, deletion of miR-183 and miR-96 (*Mir183/96*^{dko}) [12] or the whole miR-186/96/182 cluster [13, 14] does not lead to auditory dysfunction in heterozygosis. Therefore, the phenotype observed in the *Mir96*^{Dmdo} and *Mir96*$^{+14C>A}$ heterozygotes is likely to be partly due to the acquisition of new targets by the mutant miRNA.

Mice homozygous for all the *Mir96* alleles reported so far show no ABR responses at all ages tested (Table 1). This indicates that the abnormal targeting pattern of miR-96 in mutants affects the development of the hair cells, as previously described [10].

Stereocilia bundles and ribbon synapses in *Mir96*$^{+13G>A}$ and *Mir96*$^{+14C>A}$ mice

Similar to the physiological phenotype, the structural phenotype of *Mir96*$^{+13G>A}$ is much less severe than that of *Mir96*$^{+14C>A}$ and *Mir96*^{Dmdo}. Both inner and outer hair cells of *Mir96*$^{+13G>A}$ homozygotes show degenerative changes at 4 weeks old, but this phenotype is more severe in *Mir96*$^{+14C>A}$ homozygotes, where the stereocilia bundles are more severely affected by 4 weeks old (Fig. 4), and even more severe in *Mir96*^{Dmdo} homozygous mice, with very few stereocilia bundles visible in the organ of Corti at 4 weeks postnatal [4]. In *Mir183/96*^{dko} homozygous mice, hair cells are also severely affected at 4 weeks of age, with many hair bundles missing entirely. Where present, the stereocilia bundles of both OHCs and IHCs show splaying and fusion [12] (Table 1).

In *Mir96*$^{+13G>A}$ heterozygotes, a loss of some stereocilia in the shortest row of the OHC bundles was observed at 4 weeks old, when ABR thresholds were normal (Fig. 4). Several cases of cochlear defects associated with normal ABR thresholds have been reported. For example, synaptic damage in the inner ear, also referred to as cochlear synaptopathy, can produce difficulties in understanding hearing speech in noisy environments without an

increase in ABR thresholds (also known as hidden hearing loss) both after noise exposure [49] and ageing [50]. Hidden hearing loss has also been linked to auditory nerve myelination defects [51] and auditory nerve dysfunction [52]. Furthermore, it has been reported that stereocilia tip tapering can also be associated with normal ABR thresholds [53]. Our observations suggest that the loss of stereocilia in the shortest row of the OHC bundles is an additional cochlear defect that can be hidden behind normal ABR thresholds.

Similarly to *Mir96*$^{+14C>A}$ heterozygous mice, *Mir96*^{Dmdo} and *Mir183/96*^{dko} heterozygotes have rounded OHC stereocilia bundles (Fig. 4) [4, 12]. In *Mir96*$^{+14C>A}$ and *Mir96*^{Dmdo} heterozygotes, the structural phenotype correlates with the progressive hearing loss observed in these mutants. However, *Mir183/96*^{dko} heterozygotes have normal hearing.

In *Mir96*$^{+13G>A}$ homozygotes, we found significantly fewer colocalised pre- and postsynaptic densities per IHC, indicating synaptic defects (Fig. 5, Table 1). This was not observed in *Mir96*$^{+14C>A}$ homozygotes, suggesting that the mechanism of hearing loss caused by the two different mutations in *Mir96* is different. A reduced number of ribbon synapses per IHC was also observed in *Mir183/96*^{dko} homozygotes [12], and *Mir96*^{Dmdo} homozygotes exhibit immature IHC ribbon shapes and disorganised innervation [10], although in this last mutant the synapses were not quantified in the same way so cannot be directly compared.

Transcriptomic changes in *Mir96*$^{+13G>A}$ and *Mir96*$^{+14C>A}$ mutants

We have previously shown that many genes are dysregulated in *Mir96*^{Dmdo} mice as a result of the point mutation affecting the seed region, indicating that miR-96 controls a complex network of genes in the inner ear [4, 15]. In the present study, we found 328 differentially expressed genes in *Mir96*$^{+13G>A}$ homozygotes and 693 in *Mir96*$^{+14C>A}$ homozygotes. RNA-seq of *Mir183/96*^{dko} homozygotes revealed only 34 DEGs [12] and microarray performed in *Mir96*^{Dmdo} revealed 86 DEGs [4]. The milder effects observed in the knockout allele compared with point mutations in *Mir96* indicates that the gain of novel targets can play an important role in the phenotype caused by a microRNA mutation, as suggested by the Sylamer analysis (Fig. 8). We conclude that the differentially expressed genes in *Mir96*$^{+13G>A}$ and *Mir96*$^{+14C>A}$ mutant mice are related to specific pathways and cellular processes that may be responsible for the phenotypes observed by SEM and confocal microscopy.

Many DEGs (124) were shared between *Mir96*$^{+13G>A}$ homozygotes and *Mir96*$^{+14C>A}$ homozygotes (Fig. 7, Additional file 4: Table S3), but only 6 were shared between all four *Mir96* mutants (Fig. 9). This may in part be due to the different platforms used; the *Mir96*^{Dmdo} data comes from a microarray and not RNA-Seq, and many genes were not represented on the microarray. It is also worth noting that *Mir96*^{Dmdo} mice are on a C3HeB/FeJ genetic background, while *Mir96*$^{+13G>A}$, *Mir96*$^{+14C>A}$ and *Mir183/96*^{dko} mice are on a C57BL/6N background, which could explain some of the differences observed between the different mutants (Table 1). However, it is likely that much of the difference is due to the different mutations (three point mutations which affect targeting and one knockout which includes the neighbouring *Mir183* gene).

Identifying wildtype miR-96 targets

We made use of three different methods to identify potential targets of miR-96, but did not find any consistently identified candidates. It is possible that miR-96 operates mainly through mild downregulation of many direct targets, rather than strongly downregulating one or two, and thus it would be hard to identify individual target genes. One limitation of this study is that we carried out bulk RNA-seq of the whole organ of Corti, while miR-96 is only expressed in the hair cells. Therefore, if a target is highly expressed in the non-sensory epithelial cells, any difference in expression between *Mir96* wildtypes and homozygotes as a result of the repression in the hair cells might not be detectable. This might also explain why some genes that are known direct targets of miR-96, such as *Zeb1*, *Foxo1* and *Nr3c1*, are not significantly misregulated in our transcriptomic data. Single-cell RNA sequencing (scRNA-seq) would be required to approach this problem.

It is also possible that miR-96 is regulating different genes in the inner and outer hair cells because the regulation is dependent on the mRNA molecules being expressed on a specific cell type. For instance, *Ocm* and *Slc26a5*, two of the most significantly downregulated genes, are predominantly expressed in outer hair cells. This would further complicate target identification. Again, scRNA-seq would help distinguish cell type-specific regulation.

Gain of novel targets of mutant miR-96

The *Mir183/96* knockout mouse mutant (*Mir183/96*^{dko}) provides a good comparison to study only the effects of the loss of normal miR-96 targets (since *Mir96* and *Mir183* are very closely linked, it was not possible to target either gene alone [54]).

The lower number of DEGs obtained in the mice with the null allele (*Mir183/96*^{dko}) compared to the mutants with a point mutation in the seed region of miR-96 suggests that the gain of novel target mRNAs is important

for the phenotype of these mutants. Sylamer analyses [30] (Fig. 8) supported that some of the wildtype miR-96 targets were upregulated in both mutants. However, there was also a marked negative peak for heptamers matching the mutant seed regions (Fig. 8), meaning that some of the significantly downregulated genes bore matches to the mutant seed region in their 3′UTRs, and their downregulation is likely due to the acquisition of new targets by the mutant microRNA. The differences between the four *Mir96* mutants (Table 1) clearly demonstrate that the gain of novel targets plays an important role in the phenotype resulting from a point mutation in *Mir96*.

Pharmacological interventions to maintain hearing: a proof of concept

Rather than focus on a single target, because our analyses suggest that miR-96 operates through a multitude of target genes, we used the whole transcriptome to identify drugs which have the opposite effect on differential gene expression to that caused by mutant miR-96. We chose amitriptyline to test and found that it delays the progression of hearing impairment in *Mir96*$^{+14C>A}$ heterozygotes (Fig. 10). This is a proof of concept rather than a suggestion that amitriptyline be used as a treatment for humans carrying the *MIR96*$^{+14C>A}$ mutation, for several reasons. First, the dosage in mice (by body weight) was far higher than the standard amitriptyline dose used in humans; second, amitriptyline can have multiple unpleasant side effects; and third, the delay in progression of hearing loss was only temporary. However, this shows that it is possible to intervene pharmaceutically to delay hearing loss caused by a genetic defect. Currently there are no therapeutics for treating progressive hearing loss, so this is an important proof of principle. Prevention of hearing loss by CRISPR correction of the *Mir96*$^{+14C>A}$ mutation has recently been demonstrated to be effective in mice [55], but in vivo gene editing to treat hearing impairment has yet to be implemented in humans and requires precise knowledge of the underlying genetic pathology. We chose to work on *Mir96* because it is a master regulator of hair cell maturation and function, and we hypothesised that pharmaceutical interventions which help in the case of *Mir96* mutations may be more generically effective for people whose hearing loss is caused by mutations in one or some of the many genes controlled by miR-96.

It is also worth noting that we were able to find a candidate therapeutic which had an effect even without a full understanding of the complex regulatory network controlled by miR-96, and this approach may generalise to other conditions and diseases caused by mutations in regulatory molecules.

Conclusions

Here we have presented our detailed phenotypic characterisation of mice bearing human mutations in *Mir96*. While both mutants exhibit hearing impairment, the differences in the underlying pathology emphasise the importance of the gain of novel targets in the phenotypes caused by microRNA mutations. We have also demonstrated the use of transcriptome data to identify potential pharmacological interventions to maintain hearing, an important proof of concept for the development of treatments for a complex, heterogeneous condition like progressive hearing loss.

Abbreviations

ABR	Auditory brainstem response
P	Postnatal day
OTOTO	Osmium tetroxide-thiocarbohydrazide method
PFA	Paraformaldehyde
RT	Room temperature
EDTA	Ethylenediaminetetraacetic acid
IHC	Inner hair cell
OHC	Outer hair cell
UTR	Untranslated region
GSEA	Gene set enrichment analysis
FDR	False discovery rate
SEM	Scanning electron microscopy
DEG	Differentially expression gene
IPA	Ingenuity Pathway Analysis
SPIED	Searchable Platform-Independent Expression Database

Supplementary Information

The online version contains supplementary material available at https://doi.org/10.1186/s13073-024-01394-5.

Additional file 1: Table S1. Differential gene expression in Mir96 +*13G>A* homozygotes. RNA-seq results showing gene expression in Mir96 +*13G>A* homozygotes as log 2 fold change (log 2 FC) compared to sex-matched wildtype littermates. Genes are ordered by false discovery rate (FDR); unadjusted p values are also shown.

Additional file 2: Table S2. Differential gene expression in Mir96 +*14C>A* homozygotes. RNA-seq results showing gene expression in Mir96 +*14C>A* homozygotes as log 2 fold change (log 2 FC) compared to sex-matched wildtype littermates. Genes are ordered by false discovery rate (FDR); unadjusted p values are also shown.

Additional file 3: Supplementary Figures S1–S4.

Additional file 4: Table S3. 127 genes were significantly differentially expressed in both Mir96 +*13G>A* and Mir96 +*14C>A* homozygotes. Eighty-four were upregulated, 40 were downregulated, and 3 were upregulated in Mir96 +*14C>A* homozygotes and downregulated in Mir96 +*13G>A* homozygotes. Two hundred and one DEGs were unique to Mir96 +*13G>A* homozygotes, and 566 DEGs were unique to Mir96 +*14C>A* homozygotes. Only genes with significant differential expression (FDR < 0.05) are shown.

Additional file 5: Table S4. Gene sets enriched in up- and downregulated genes in Mir96 +*13G>A* and Mir96 +*14C>A* homozygotes. For each gene set, the number of the genes present in the RNA-seq dataset is shown, along with enrichment score (which indicates the degree of overrepresentation of the gene set at the top or the bottom of the list of input genes ranked by differential expression), normalised enrichment score (which accounts for gene set size), p value (significance of enrichment score for the single gene set) and false discovery rate (FDR; the probability that a gene set with that normalised enrichment score represents a false positive finding, corrected for multiple testing and gene

set size). Gene sets are ordered by FDR. Two gene sets corresponding to predicted miR-96 targets are enriched in upregulated genes in the Mir96 + 13G > A transcriptome, but neither are enriched in the Mir96 + 14C > A transcriptome, which means that the genes in those gene sets are relatively evenly distributed through the Mir96 + 14C > A RNA-seq gene list when ranked by differential expression. This could be due to the much greater number of significantly misregulated genes in the Mir96 +*14C>A* transcriptome, which may mask the signal from the loss of the wildtype miR-96 targeting.

Additional file 6: Table S5. Significant pathways from Ingenuity Pathway Analysis. The z-score is a measure of the predicted activity (for positive z-scores) or inhibition (for negative z-scores) of the pathway, based on the known misregulation of the differentially expressed genes in that pathway.

Additional file 7: Table S6. Candidate direct targets identified from the transcriptomes of four Mir96 mutant mice using three different methods.

Additional file 8: Table S7. Gene sets enriched in up- and downregulated genes in Mir96 *Dmdo* and Mir183/96 *dko* homozygotes. For each gene set, the number of the misregulated genes from the RNA-seq analysis is shown, along with enrichment score (based on the number of misregulated genes in the gene set, the total number of misregulated genes and the overall gene set size), normalised enrichment score (which accounts for gene set size), p value (significance of enrichment score for the single gene set) and false discovery rate (FDR; the probability that a gene set with that normalised enrichment score represents a false positive finding, corrected for multiple testing and gene set size). Gene sets are ordered by FDR. Transcriptome data are from [4] and [12].

Additional file 9: Table S8. Input and output from the SPIED tool. The transcriptomes from Mir96 +*13G>A* and Mir96 +*14C>A* homozygotes were combined by excluding genes misregulated in opposite directions. The resulting list, used as input for SPIED, is shown on the left sub-table. The SPIED output for this list is shown in the middle sub-table, and the SPIED output for the Mir183/96 *dko* transcriptome alone [12] is shown in the right sub-table. Output columns show the compound, tissue and stage of each correlated or anti-correlated DrugMatrix expression profile, the correlation score of the input transcriptome data with that DrugMatrix expression profile, the z-score of that correlation (the highest z-score is the best-correlated profile) and the number of genes from the input transcriptome present in the DrugMatrix expression profile.

Additional file 10: Data S1. Data underlying the graphs and charts presented in this study.

Acknowledgements
We thank Flavia Davidhi, Jack Blackburn and Susana Caetano for technical support, Neil Ingham for maintaining the auditory physiology facility and the King's College London Centre for Ultrastructural Imaging for maintaining the electron microscopy facility.

Authors' contributions
MAL carried out the electrophysiology, noise exposure, and drug administration, collection and dissection of P4 samples and RNA extraction, design and implementation of the RNA-seq analysis pipeline, and the Sylamer, IPA and SPIED analyses. MLR carried out the confocal microscopy and synapse quantification, RNA extraction, cDNA creation and qPCR, and the gene set enrichment analysis of the RNA-seq data. FDD and JC carried out the scanning electron microscopy. GD created the knock-in mice. SF contributed to the design of the bioinformatic pipeline and GW helped carry out the SPIED analysis. MAL, MM, MAMP and KPS obtained the funding. KPS and MAMP supervised the research. The paper was written by MLR, MAL and KPS. All authors read and approved the final manuscript.

Funding
This work was supported by the Royal National Institute for Deaf People (RNID) (G88 to MAL and KPS) and Wellcome (221769/Z/20/Z and WT089622MA to KPS). We thank the Wellcome Sanger Institute Mouse Genetics Project for supporting the production of the two *Mir96* mutants (098051). The work has also received funding from the Regional Government of Madrid (B2017/BMD3721 to MAM-P) and from Instituto de Salud Carlos III, cofounded with the European Regional Development Fund "A way to make Europe" within the National Plans for Scientific and Technical Research and Innovation 2017–2020 and 2021–2024 (PI20/0429, PI23-1534 and IMP/00009 to MAM-P). This research was funded in part by the Wellcome Trust. For the purpose of Open Access, the author has applied a CC BY public copyright licence to any Author Accepted Manuscript (AAM) version arising from this submission.

Data availability
Transcriptome data from the two mouse mutants reported here are publicly available from ArrayExpress, accession number E-MTAB-13772 (https://www.ebi.ac.uk/biostudies/arrayexpress/studies/E-MTAB-13772) [56]. All other datasets are included in this article and its supplementary information files. Both mouse lines are available through the European Mouse Mutant Archive (EMMA) (*Mir96*$^{+13G>A}$: EM:14179 (https://www.infrafrontier.eu/emma/strain-search/straindetails/?q=14179); *Mir96*$^{+14C>A}$: EM:11885 (https://www.infrafrontier.eu/emma/strain-search/straindetails/?q=11885)).

Declarations

Ethics approval and consent to participate
Mouse studies were performed in compliance with UK Home Office regulations and the Animals (Scientific Procedures) Act of 1986 (ASPA) under UK Home Office licencing, and the study was approved by the King's College London Ethical Review Committee. Mice were culled using methods permitted under these licences to minimise any possibility of suffering.

Consent for publication
Not applicable.

Competing interests
The authors declare they have no competing interests.

Received: 7 March 2024 Accepted: 9 October 2024
Published online: 21 October 2024

References

1. Cherny SS, Livshits G, Wells HRR, Freidin MB, Malkin I, Dawson SJ, et al. Self-reported hearing loss questions provide a good measure for genetic studies: a polygenic risk score analysis from UK Biobank. Eur J Hum Genet. 2020;28(8):1056–65.
2. Wingfield A, Panizzon M, Grant MD, Toomey R, Kremen WS, Franz CE, et al. A twin-study of genetic contributions to hearing acuity in late middle age. J Gerontol A Biol Sci Med Sci. 2007;62(11):1294–9.
3. Wolber LE, Steves CJ, Spector TD, Williams FM. Hearing ability with age in northern European women: a new web-based approach to genetic studies. PLoS ONE. 2012;7(4): e35500.
4. Lewis MA, Quint E, Glazier AM, Fuchs H, De Angelis MH, Langford C, et al. An ENU-induced mutation of miR-96 associated with progressive hearing loss in mice. Nat Genet. 2009;41(5):614–8.
5. Mencia A, Modamio-Hoybjor S, Redshaw N, Morin M, Mayo-Merino F, Olavarrieta L, et al. Mutations in the seed region of human miR-96 are responsible for nonsyndromic progressive hearing loss. Nat Genet. 2009;41(5):609–13.
6. Solda G, Robusto M, Primignani P, Castorina P, Benzoni E, Cesarani A, et al. A novel mutation within the MIR96 gene causes non-syndromic inherited hearing loss in an Italian family by altering pre-miRNA processing. Hum Mol Genet. 2012;21(3):577–85.
7. Bartel DP. MicroRNAs: genomics, biogenesis, mechanism, and function. Cell. 2004;116(2):281–97.
8. Winter J, Jung S, Keller S, Gregory RI, Diederichs S. Many roads to maturity: microRNA biogenesis pathways and their regulation. Nat Cell Biol. 2009;11(3):228–34.
9. Lewis BP, Burge CB, Bartel DP. Conserved seed pairing, often flanked by adenosines, indicates that thousands of human genes are microRNA targets. Cell. 2005;120(1):15–20.

10. Kuhn S, Johnson SL, Furness DN, Chen J, Ingham N, Hilton JM, et al. miR-96 regulates the progression of differentiation in mammalian cochlear inner and outer hair cells. Proc Natl Acad Sci USA. 2011;108(6):2355–60.
11. Schluter T, Berger C, Rosengauer E, Fieth P, Krohs C, Ushakov K, et al. miR-96 is required for normal development of the auditory hindbrain. Hum Mol Genet. 2018;27(5):860–74.
12. Lewis MA, Di Domenico F, Ingham NJ, Prosser HM, Steel KP. Hearing impairment due to Mir183/96/182 mutations suggests both loss and gain of function effects. Dis Model Mech. 2020;14(2):dmm047225.
13. Fan J, Jia L, Li Y, Ebrahim S, May-Simera H, Wood A, et al. Maturation arrest in early postnatal sensory receptors by deletion of the miR-183/96/182 cluster in mouse. Proc Natl Acad Sci USA. 2017;114(21):E4271–80.
14. Geng R, Furness DN, Muraleedharan CK, Zhang J, Dabdoub A, Lin V, et al. The microRNA-183/96/182 cluster is essential for stereociliary bundle formation and function of cochlear sensory hair cells. Sci Rep. 2018;8(1):18022.
15. Lewis MA, Buniello A, Hilton JM, Zhu F, Zhang WI, Evans S, et al. Exploring regulatory networks of miR-96 in the developing inner ear. Sci Rep. 2016;6:23363.
16. Modamio-Hoybjor S, Moreno-Pelayo MA, Mencia A, del Castillo I, Chardenoux S, Morais D, et al. A novel locus for autosomal dominant nonsyndromic hearing loss, DFNA50, maps to chromosome 7q32 between the DFNB17 and DFNB13 deafness loci. J Med Genet. 2004;41(2):e14.
17. Ingham NJ, Pearson S, Steel KP. Using the auditory brainstem response (ABR) to determine sensitivity of hearing in mutant mice. Current protocols in mouse biology. 2011;1(2):279–87.
18. Holme RH, Steel KP. Progressive hearing loss and increased susceptibility to noise-induced hearing loss in mice carrying a Cdh23 but not a Myo7a mutation. J Assoc Res Otolaryngol. 2004;5(1):66–79.
19. Ingham NJ, Rook V, Di Domenico F, James E, Lewis MA, Girotto G, et al. Functional analysis of candidate genes from genome-wide association studies of hearing. Hear Res. 2020;387: 107879.
20. Hunter-Duvar IM. A technique for preparation of cochlear specimens for assessment with the scanning electron microscope. Acto Otoloaryng Suppl. 1978;351:3–23.
21. Muller M, von Hunerbein K, Hoidis S, Smolders JW. A physiological place-frequency map of the cochlea in the CBA/J mouse. Hear Res. 2005;202(1–2):63–73.
22. Eaton-Peabody Laboratories Histology Core. https://www.masseyeandear.org/research/otolaryngology/eaton-peabody-laboratories/histology-core. Accessed 26 Feb 2024.
23. Livak KJ, Schmittgen TD. Analysis of relative gene expression data using real-time quantitative PCR and the 2(T)(-delta delta C) method. Methods. 2001;25(4):402–8.
24. Bermingham-McDonogh O, Oesterle EC, Stone JS, Hume CR, Huynh HM, Hayashi T. Expression of Prox1 during mouse cochlear development. J Comp Neurol. 2006;496(2):172–86.
25. FAST-X Toolkit. http://hannonlab.cshl.edu/fastx_toolkit/index.html. Accessed 2023.
26. Kim D, Langmead B, Salzberg SL. HISAT: a fast spliced aligner with low memory requirements. Nat Methods. 2015;12(4):357–60.
27. Danecek P, Bonfield JK, Liddle J, Marshall J, Ohan V, Pollard MO, et al. Twelve years of SAMtools and BCFtools. Gigascience. 2021;10(2):giab008.
28. Anders S, Pyl PT, Huber W. HTSeq—a Python framework to work with high-throughput sequencing data. Bioinformatics. 2015;31(2):166–9.
29. Robinson MD, McCarthy DJ, Smyth GK. edgeR: a Bioconductor package for differential expression analysis of digital gene expression data. Bioinformatics. 2010;26(1):139–40.
30. van Dongen S, Abreu-Goodger C, Enright AJ. Detecting microRNA binding and siRNA off-target effects from expression data. Nat Methods. 2008;5(12):1023–5.
31. Mootha VK, Lindgren CM, Eriksson KF, Subramanian A, Sihag S, Lehar J, et al. PGC-1alpha-responsive genes involved in oxidative phosphorylation are coordinately downregulated in human diabetes. Nat Genet. 2003;34(3):267–73.
32. Subramanian A, Tamayo P, Mootha VK, Mukherjee S, Ebert BL, Gillette MA, et al. Gene set enrichment analysis: a knowledge-based approach for interpreting genome-wide expression profiles. Proc Natl Acad Sci USA. 2005;102(43):15545–50.
33. Molecular Signature Database (MSigDB v7.1). https://www.gsea-msigdb.org/gsea/msigdb/index.jsp. Accessed 8 Dec 2022.
34. Reimand J, Isserlin R, Voisin V, Kucera M, Tannus-Lopes C, Rostamianfar A, et al. Pathway enrichment analysis and visualization of omics data using g:Profiler, GSEA, Cytoscape and EnrichmentMap. Nat Protoc. 2019;14(2):482–517.
35. Caldarone BJ, Karthigeyan K, Harrist A, Hunsberger JG, Wittmack E, King SL, et al. Sex differences in response to oral amitriptyline in three animal models of depression in C57BL/6J mice. Psychopharmacology. 2003;170(1):94–101.
36. Bridge PD, Sawilowsky SS. Increasing physicians' awareness of the impact of statistics on research outcomes: comparative power of the t-test and Wilcoxon rank-sum test in small samples applied research. J Clin Epidemiol. 1999;52(3):229–35.
37. Duricki DA, Soleman S, Moon LD. Analysis of longitudinal data from animals with missing values using SPSS. Nat Protoc. 2016;11(6):1112–29.
38. Krueger C, Tian L. A comparison of the general linear mixed model and repeated measures ANOVA using a dataset with multiple missing data points. Biol Res Nurs. 2004;6(2):151–7.
39. Noben-Trauth K, Zheng QY, Johnson KR. Association of cadherin 23 with polygenic inheritance and genetic modification of sensorineural hearing loss. Nat Genet. 2003;35(1):21–3.
40. Li HS, Borg E. Age-related loss of auditory sensitivity in two mouse genotypes. Acta Otolaryngol. 1991;111(5):827–34.
41. Kramer A, Green J, Pollard J Jr, Tugendreich S. Causal analysis approaches in Ingenuity Pathway Analysis. Bioinformatics. 2014;30(4):523–30.
42. DrugMatrix/ToxFX. https://ntp.niehs.nih.gov/data/drugmatrix. Accessed 2023.
43. Williams G. SPIED3: a searchable platform-independent expression database. https://www.spied.org.uk. Accessed 15 Dec 2023.
44. Williams G. A searchable cross-platform gene expression database reveals connections between drug treatments and disease. BMC Genomics. 2012;13: 12.
45. Williams G. SPIEDw: a searchable platform-independent expression database web tool. BMC Genomics. 2013;14(1): 765.
46. Shibata SB, Osumi Y, Yagi M, Kanda S, Kawamoto K, Kuriyama H, et al. Administration of amitriptyline attenuates noise-induced hearing loss via glial cell line-derived neurotrophic factor (GDNF) induction. Brain Res. 2007;1144:74–81.
47. Coudore F, Fialip J, Eschalier A, Lavarenne J. Plasma and brain pharmacokinetics of amitriptyline and its demethylated and hydroxylated metabolites after acute intraperitoneal injection in mice. Eur J Drug Metab Pharmacokinet. 1994;19(1):5–11.
48. Knapp L, Sun H, Wang YM, Chen BJ, Lin X, Gao N, et al. Rab11a is essential for the development and integrity of the stereocilia and kinocilia in the mammalian organ of Corti. eNeuro. 2023;10(6):ENEURO.0420-22.
49. Kujawa SG, Liberman MC. Adding insult to injury: cochlear nerve degeneration after "temporary" noise-induced hearing loss. J Neurosci. 2009;29(45):14077–85.
50. Sergeyenko Y, Lall K, Liberman MC, Kujawa SG. Age-related cochlear synaptopathy: an early-onset contributor to auditory functional decline. J Neurosci. 2013;33(34):13686–94.
51. Wan G, Corfas G. Transient auditory nerve demyelination as a new mechanism for hidden hearing loss. Nat Commun. 2017;8: 14487.
52. Reijntjes DOJ, Lee JH, Park S, Schubert NMA, van Tuinen M, Vijayakumar S, et al. Sodium-activated potassium channels shape peripheral auditory function and activity of the primary auditory neurons in mice. Sci Rep. 2019;9(1):2573.
53. Ingham NJ, Banafshe N, Panganiban C, Crunden JL, Chen J, Lewis MA, et al. Inner hair cell dysfunction in Klhl18 mutant mice leads to low frequency progressive hearing loss. PLoS ONE. 2021;16(10): e0258158.
54. Prosser HM, Koike-Yusa H, Cooper JD, Law FC, Bradley A. A resource of vectors and ES cells for targeted deletion of microRNAs in mice. Nat Biotechnol. 2011;29(9):840–5.
55. Zhu W, Du W, Rameshbabu AP, Armstrong AM, Silver S, Kim Y, et al. Targeted genome editing restores auditory function in adult mice with progressive hearing loss caused by a human microRNA mutation. Sci Transl Med. 2024;16(755):eadn0689.
56. Lewis MA, Lachgar-Ruiz M, Di Domenico F, Duddy G, Chen J, Fernandez S, et al. RNAseq of organ of Corti RNA from mice carrying human mutations in Mir96. E-MTAB-13772, ArrayExpress. 2024. https://www.ebi.ac.uk/biostudies/arrayexpress/studies/E-MTAB-13772.

Publisher's Note

Springer Nature remains neutral with regard to jurisdictional claims in published maps and institutional affiliations.